AN ABSTRACT OF THE CAPSTONE REPORT OF

Natalie Schibrowsky for the degree of Masters of Chemical Sciences

Title: Molecular mechanism of copper regulation of mitogen-activated protein kinase (MEK1)

Project conducted at: University of Pennsylvania,
BRB II/III, Room 432, 421 Curie Blvd, Philadelphia, PA 19104-6101
Supervisor: *Prof. Ronen Marmorstein*
Dates of Project: May 2, 2016 – May 10, 2017
Abstract approved: *Prof. Ronen Marmorstein*, Academic Advisor

Mutated constitutively activated forms of the BRAF kinase have been associated with various cancers, such as melanoma and leukemia. One such common BRAF mutant, $BRAF^{V600E}$ is found in about 50% of melanomas. BRAF is part of the MAPK signaling cascade that contains the downstream target MEK1/2, which phosphorylates ERK1/2 and subsequently increases cell proliferation. While the majority of the therapeutic inhibitors of the MAPK pathway have been designed to target BRAF, some have also targeted MEK1/2 as well as other kinases within the pathway such as ERK1/2. Recently, MEK1 has been observed to interact with copper (Cu). This element and copper transporter 1 (CTR1) were found to be important for kinase activity and when absent, decreased the ability of $BRAF^{V600E}$ to signal and mediate tumorigenesis. In this study, work was done to further characterize the MEK1-Cu interaction through crystallography, and carried out associated biochemical and enzymatic studies in order to characterize the functional consequence of the interaction and its effects on downstream ERK phosphorylation. A crystal structure of a MEK1-Cu complex was obtained revealing a Cu binding site to a regulatory site of the kinase that would be predicted to inhibit kinase activity. This structural observation is supported by functional studies with bacterially produced recombinant homogeneously purified MEK1 demonstrating that Cu inhibits MEK1 kinase activity *in vitro*. Interestingly, crudely purified MEK1 did show Cu-mediated MEK1 activation suggesting another mode of Cu-mediated MEK1 activation that is yet to be characterized. These results suggest that MEK1 is a metal-sensitive enzyme and that targeting these metals may be exploited to inhibit MAPK signaling for therapy.

Molecular mechanism of copper regulation of
mitogen-activated protein kinase (MEK1)
by
Natalie Schibrowsky

A CAPSTONE REPORT

submitted to the

University of Pennsylvania

in partial fulfillment of
the requirements for
the degree of

Masters of Chemical Sciences

Presented (*May 10, 2017*)
Commencement (*May 15, 2017*)

Master of Chemical Sciences Capstone Report of *Natalie A. Schibrowsky* presented on May 10, 2017

APPROVED:

Ronen Marmorstein, representing *Biological Chemistry*

I understand that my Capstone Report will become part of the permanent collection of the University of Pennsylvania Master of Chemical Sciences Program. My signature below authorizes release of my final report to any reader upon request.

Natalie A. Schibrowsky, Author

Acknowledgements

There are (quite) a few people I would like to thank for their help and support during my research and time in the Masters of Chemical Sciences program.

The first step of being a graduate student is being a part of a program, which I would like to thank Dr. Ana-Rita Mayol-Cabassa for the acceptance into the MCS program, committee participation, and teachings. All of her lectures (that seemed redundant at the time) and intense assignments (the brutal ACS citation assignment will never be forgotten) have helped me to develop more scientific skills and polish my professional skill set as well.

The next step in being a *successful* graduate student is a solid foundation, which I would like to thank Dr. Ronen Marmorstein. Dr. Marmorstein has been a phenomenal PI and even with a large lab, shows each and every student respect and individual attention to their projects. I thank him for his collaboration with Dr. Donita Brady, which has given me an amazing research opportunity for my capstone. Through the countless papers, reviews, and presentations/posters (specifically the revisions and feedback), I have learned more than I thought possible, which I am indebted and eternally grateful. His genuine interest and concern for obtaining answers to real world problems have inspired me even more to continue to pursue a career in academia to hopefully have a similar impact on the next generation of scientists. I could expect nothing less from such a phenomenal PI to have such an outstanding lab. He has created a unique lab dynamic of hardworking, driven, welcoming, knowledgeable, and personable students that are true representations of the University of Pennsylvania culture. The bullpen includes: Adam Olia, Joe Han, Dan Ricketts, Rob Magin, Julie Barber-Rotenberg, Gleb Bazilevsky, Leah Gottlieb, Austin Vogt, Angel Pagan, Michael Shin, Ryan Emptage, Elliot Dean, Sunbin Deng, Marianne Goris, Kevin DAmico, and Mike Grasso. I will definitely miss Adam's crazy, bizarre scientific suggestions that always have underlying plausibility of whether or not they will fix the problem; Kevin for somehow keeping the lab afloat as everything broke within a two and a half month time period; Rob's interesting, yet culturally informing conversations, especially with Marianne; and Angel and Michael wandering around lab together. Above all else, I need to thank Mike Grasso for being my mentor in lab and teaching me pretty much everything I know. I would have been lost without him, so I thank him from the bottom of my heart for teaching, celebrating, laughing, and sometimes suffering with me through my time here. I will never be able to replace him as a Bay Mate or his teenage girl music playlist.

The third and final thing to be a successful graduate student is a strong support system that sees you through all of the highs and the lows. The people who will comfort you in your times of need and make you coffee (or buy me Starbucks) after an all-nighter. This includes my mother and father Angel and Jack Schibrowsky; the love of my life Daniel Tafoya and his family, doggo, and pupper; my aunt Natalie, cousins Alexa and Alyssa, and godfamily Nicholas and Carmen Canaii; all my friends from UNLV; my biggest supporter and inspiration Dr. Ralph Conti; Jiale Huang for being the best, most supportive, and one of my truest friends; The Huge, the Enormous, the Well-Endowed, Undefeated, Ivy-League Champion, University of Pennsylvania Oxymoronic Fighting Quaker Marching Band, Greer Cheeseman, Adam Sherr, and Mr. Dr. Kushol Gupta, Ph.D. Shoutouts go to Richard DiNapoli and Nikolas Alvelo for being my best marching band geek buddies I could ask for in a scramble band; Miranda Somich, Giulia Arostegui, and Matt Eisenberg for being the closest bass line family that I love so much; Derek Arbige, Jeanette Freeman, Ana Cohen, Joe Klinger, Emily Elenio, Cathy Zhang, Laura Kuder, Zabryna Atkinson-Diaz, Jackie Valeri, and Ben Parker (impeach!) for always making me laugh or smile whether they knew it or not; the (almost undefeated) Quizzo squad led by Aaron Mittleman, Hannah Salazar, and Jackson Betz; and Kyle McKee and Jenna Harowitz for being amazing drum majors and teachers in the special art of arm waving.

Thank you all for everything! <3 Without further ado, let the real science commence.

Table of Contents

List of Figures

List of Tables

List of Appendices

Introduction

Importance & Significance

Cancer is a class of diseases that cause unregulated division of abnormal cells within different body systems or organs. It is one of the most potent classes of diseases, since an overall cure has yet to be discovered. In response to this, many labs have dedicated their research to understanding the molecular underpinnings of cancer in order to develop effective therapies. Cancer can result in the mutational activation of cellular lines of communication that drive cellular proliferation. Since cancers are caused by different underlying abnormalities, cellular pathways and macromolecules must be studied in order to develop effective targeted therapies. Melanoma targets the skin and is mostly caused by over exposure to natural and artificial ultraviolet rays, but has also been tied to a combination of genetics and other environmental factors.[1] Since melanoma incidence is steadily rising, with mortality rates of 1 in 8 people in the last decade, it is imperative to find effective treatments for the projected 144,000 people who will be diagnosed in 2016 alone.[2] This cancer exploits normal cellular signal transduction pathways to promote uncontrolled cell division, a hallmark of cancer. In a healthy individual, different enzymes and proteins communicate within signal transduction pathways to cause specific biological activities, such as cell growth and division. In normal signal transduction, the initial signal is received from the extracellular environment, and read by a membrane-bound receptor protein, which then elicits an initial intracellular event. Signaling then proceeds within the cell to modulate metabolism and gene expression programs to drive different biological pathways. However, errors or alterations of these processes cause diseases such as cancer and metabolic disorders.

Purpose & Hypothesis

This project is based on a report demonstrating that copper (Cu) is required for BRAF signaling and tumorigenesis through direct stimulation of MEK1 kinase activity.[3] The focus of this project is to on understand the molecular basis for how Cu binds and stimulates MEK1 kinase activity towards its downstream substrates (ERK1/2). There are two mechanisms that we hypothesized to be the most plausible. In one mechanism, copper could allosterically activate MEK1 for more efficient ERK1/2 phosphorylation. In a second mechanism, Cu could strengthen the interaction between MEK1 and ERK1/2, thus leading to enhanced ERK1/2 phosphorylation. This is of importance to study in order to find new methods to inhibit the kinases in this pathway responsible for cell proliferation and cancer. Since MEK1/2 are the first mammalian kinases to be found to interact with a transition metal, this study is also of general biological importance. Furthermore, the oxidation state of the Cu species interacting with MEK1 is unclear. While Cu^{+} is rare and unstable compared to Cu^{2+}, it is possible that within the phosphorylation process there is a fleeting moment where Cu^{+} is stabilized and oxidized to Cu^{2+} by the reducing environment within the cell influencing MEK1's ability to phosphorylate ERK2. While more difficult to determine, more information regarding the oxidation state of Cu on this can be elucidated through this study.

Background

MAPK Pathway

Kinases are enzymes that are responsible for phosphorylating other proteins to signal different actions. Since kinases all have the role of phosphorylation, they contain conserved motifs that mediate conserved enzymatic activities. One such conserved motif is the activation segment (loop), labeled in Figure 1a, which typically lies between a conserved Asp-Phe-Gly and Ala-Pro-Glu sequences and is typically the site of regulatory phosphorylation.[4] A Gly-rich loop is another conserved region in the amino terminal end of the kinase domain. This is a flexible loop with a consensus motif of Gly-X-Gly-X-X-Gly that locks the ATP phosphates into the catalytic site.[4] The $BRAF^{V600E}$ mutation occurs in the activation segment and causes a 500-fold increase in activation of the downstream MEK1 kinase. The V600E mutation in BRAF mimics activation loop phosphorylation of the wild-type BRAF kinase, thus rendering the kinase constitutively active for MEK1 phosphorylation.

The MAPK pathway is organized into a three-tiered kinase signaling network. The pathway of interest begins with Epidermal Growth Factor (EGF), which binds to its receptor (EGFR) on the cell membrane and leads to regulation of transcription factors within the nucleus. The canonical MAPK pathway is being studied, that includes the enzymes RAS, RAF (A, B and C isoforms) which corresponds to Tier 1 in Figure 2, MEK (MAP2K1 and MAP2K2 isoforms) which corresponds to Tier 2 in figure 2, and ERK (MAPK1 and MAPK3 isoforms) which corresponds to Tier 3 in Figure 2. Specifically, active GTP-bound RAS binds to activate the serine threonine kinase RAF. The RAF kinase then phosphorylates and activates the kinases MEK1 and MEK2. This study focused on the Tier 2 kinase in the cascade with dual specificity (MEK1) encoded by the MAP2K1 gene. This protein is also responsible for acting as an integration point, in which different signals are attached to MEK1 to allow for different responses to activate cellular processes such as proliferation and differentiation.[5] Within the MAP kinase signal transduction pathway, MEK1 is activated by many extra- and intra- cellular signals. Upon activation, it then stimulates the enzymatic activity of MAP kinases for further phosphorylation and activation of other enzymes. This type of phosphorylation is called a kinase cascade[6], where a phosphorylation event activates a kinase and then that activated kinase phosphorylates another kinase and so on (Figure 2). MEK1 then continues further downstream to the next kinase, and in mammals that is the extracellular-signal-regulated kinases (ERKs).

Extracellular-signal-regulated kinases (ERK) are protein kinase intracellular signaling molecules that are ubiquitously expressed. They are activated by various stimuli, including growth factors, cytokines, and transforming agents. Upon their activation, ERKs regulate meiosis, mitosis, and post-mitotic functions depending on the cell type. ERK2, also referred to as MAPK1, has other roles than phosphorylation within the cell, as it also activates physiological responses through nuclear translocation.[5] Nuclear translocation is simply the process of proteins or other macromolecules being transported from the cytoplasm to the nucleus. Due to translocation of Ser-Pro-Ser site, downstream acidic residues, and other elements through passive and active processes, ERK2 phosphorylates casein kinase 2 (CK2), which is responsible for regulating apoptosis.[5] Due to the combination of its growth factor effects and CK2 interaction, ERK2 has become of particular interest for anti-cancer drug design. For this reason, this

study focuses on the effects of MEK1 (Tier 2) on ERK2 (Tier 3) phosphorylation (Figure 2) with relation to different additives.

While the MAPK pathway is normally tightly controlled, several cancers exploit this pathway via kinase mutations that result in constitutive, unregulated, activation of the pathway. Upstream activation of the Receptor Tyrosine Kinases (RTKs), like EGFR, and mutations in RAS genes can cause cancer. Therefore, many of the kinases within this pathway have been studied as potential targets for inhibition for therapy. For example, ~50% of all melanoma patients have been identified to have a V600E mutated B-RAF resulting in unregulated B-RAF activation, uncontrolled cell division, and tumor growth.[7] The reason these are such prevalent drug targets is because they are driver mutations in cancer and the cells depend on them for growth. In order to effectively eliminate cancer in these patients, the MAPK pathway must be inhibited and resistance mechanisms, which often occur after therapy, must be avoided.[5]

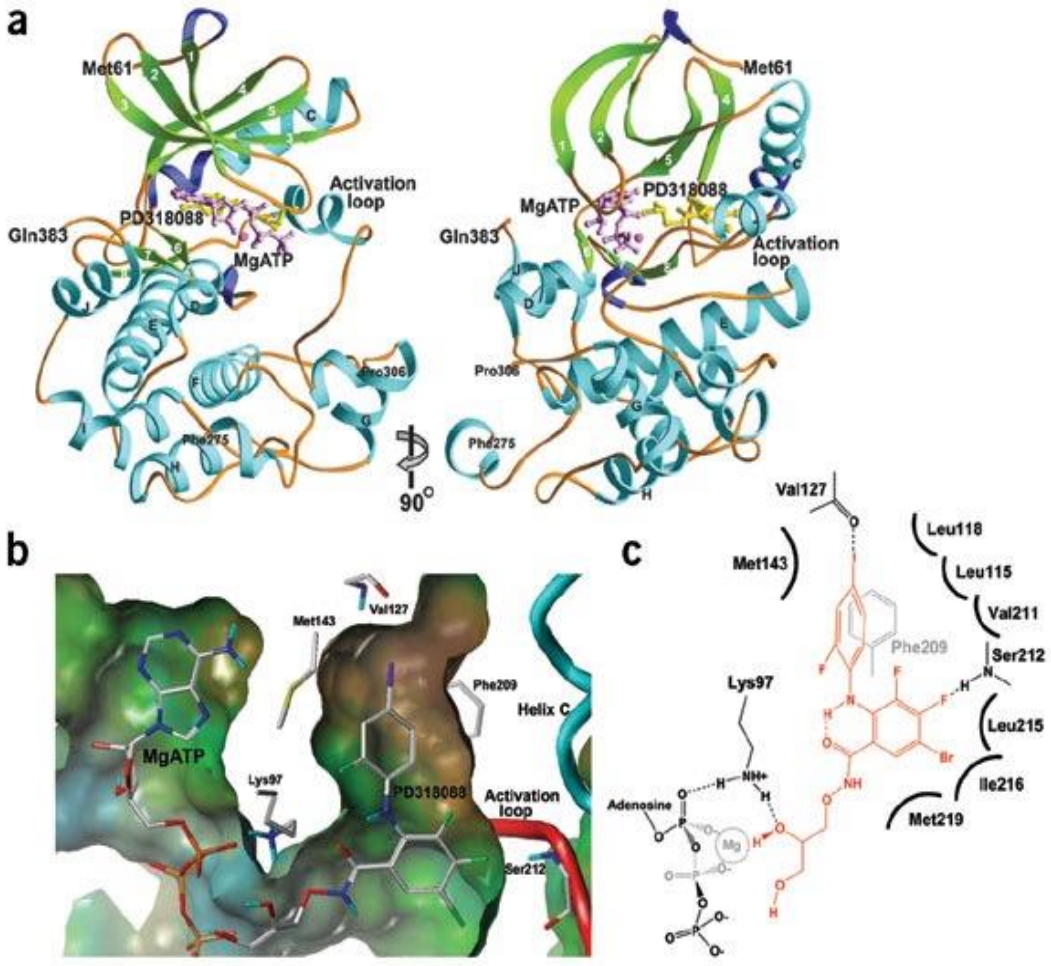

Figure 1. Structural viewpoints of MEK1's active site bound to inhibitor PD318088.[8]

Current State of MAPK Pathway Inhibition

There have been many studies reported focusing on the development of small molecule MAPK pathway inhibitors. Many of these studies have focused on targeting

RAF and MEK for inhibition. These studies have exploited information about the X-ray crystal structures of B-RAF and MEK (Figure 1) and have led to the development of several potent inhibitors that have entered clinical trials and are currently used for therapy. Current BRAF inhibitors include Vemurafenib and Dabrafenib, which disrupt the BRAF-MEK interaction and cause apoptosis within melanoma cell lines.[3] Although many patients show a positive initial response to these inhibitors, all patients develop drug resistance causing cancer relapse. Additional inhibitors have been designed to combat the relapse that occurs through paradoxical activation of BRAF[4], but more effective approaches are being researched to overcome this feedback loop. While few, MEK inhibitors include Trametinib, Cobimetnib, and MEK162, which inhibits anchorage-independent growth of Ki-Ras by blocking ERK and rapamycin-p70 pathways.[4] Due to the high efficiency of the MAPK cascade, most MEK1 inhibitors are used in combination with BRAF treatments in order to inhibit the entire pathway. While these MEK1 inhibitors are effective in combination with BRAF treatments, independent therapeutic strategies are needed. MEK1 is also involved in other cancers, such as ovarian and breast cancers, thus it needs to be further studied in order to understand the sites to target for new inhibitors.

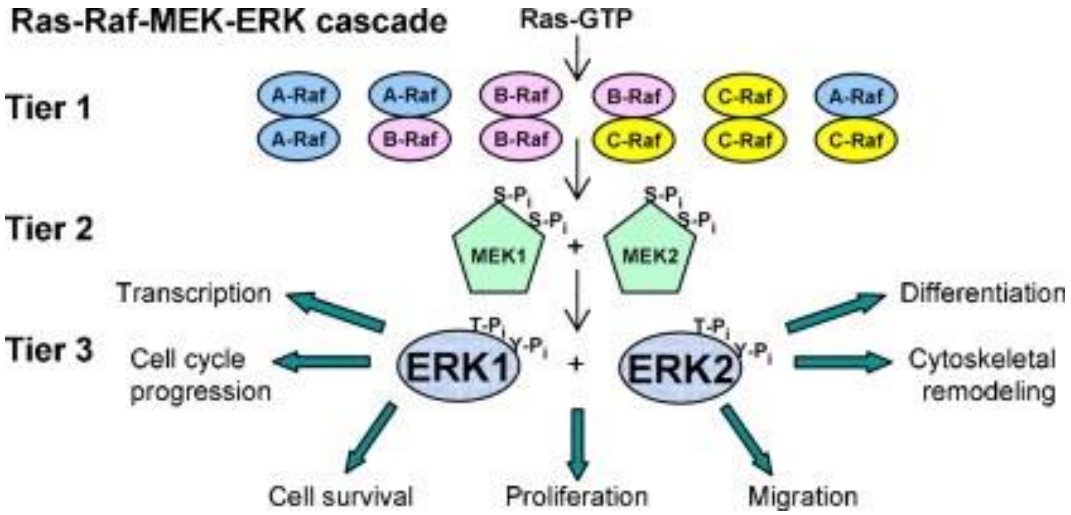

Figure 2. The canonical MAPK pathway. The P_i symbols shown on MEK1/2 and ERK1/2 symbolize phosphorylation at those residues (S or T, Y respectively).[5] The interactions for this study focus on Tier 2 (MEK1) and its interaction with Cu to phosphorylate Tier 3 (ERK2).

Studies Implicating Copper in MEK1 Activation

A recent study by Dr. Brady and colleagues discovered that an increase in copper (Cu) enhances the ability of MEK1 to phosphorylate ERK1/2.[3] The studies included testing the role of the Cu transporter 1 (Ctr1) in this process and demonstrated that decreasing the Cu concentration in mouse cells decreases the phosphorylation levels of the ERK1/2 kinases. The authors also conducted a number of studies on tumorigenesis and demonstrated that decreasing the level of Ctr1 or mutating regions of MEK1 that mediate Cu-activation of MEK1 activity inhibits tumor growth. To show the dependence of Cu's role within cells, the number of tumors was used to determine the effects of Cu with the Ctr1 gene present and absent. By removing Ctr1 with Cu present, the number of

visual tumors, shown as white arrows on Figure 3a, decreased within an excised lung (Figure 3b).[3] To confirm that not only tumors, but tumor cells were being affected by the absence of Ctr1, tumor cell percentages were studied through the quantification of a histochemical stain. Figure 3c and 3d shows a histochemical staining image. The darker pink spots correlates with abnormal/tumor lung tissue. Figure 3c shows a higher percentages of abnormal/tumor lung tissue than Figure 3d.[3] MEK1's ability to phosphorylate ERK (p-ERK) with and without Ctr1 was also tested within the tumors. The amount of p-ERK signal (red histochemical staining on Figure 3e) was greatly reduced (Figure 3f) to a point of cell "moribundity".[3] Conversely, activating the MAPK pathway in a Cu independent (no additive) fashion stimulated tumor growth (Figure 3). All of these findings combined, highlight the importance of Cu's regulation of MEK1 activity for driving the MAPK pathway and point to the inhibition of Cu-mediated MEK1 activation as a potential novel strategy to inhibit MAPK signaling in melanoma patients with the $BRAF^{V600E}$ mutation.[3]

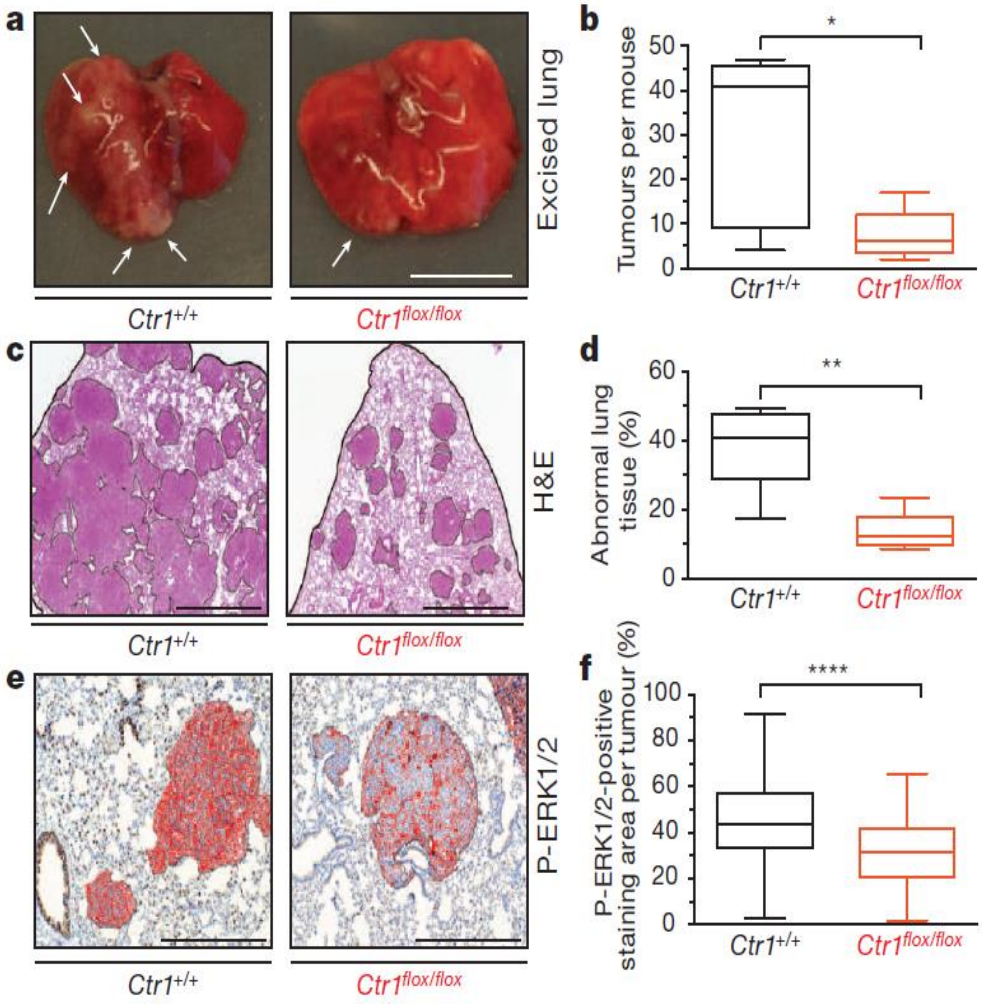

Figure 3. Histochemical tissue samples with statistical analyses of tumorous cancer cells present with respect to presence and absence of Ctr1 and pERK1/2.[3]

Given the knowledge of the MAPK pathway[1-8], evidence displaying activation with Cu^3 (Figure 3), and understanding the limitations of the current MEK inhibitors, it becomes evident that more studies are needed. This study looks to characterize the interaction between MEK1-Cu by determining the MEK1 residues and Cu oxidation state involved through crystallography. After solving the structure and determining the residues, mutagenesis can be combined with *in vitro* assays to qualitatively and quantitatively determine the influence of Cu on MEK1. These assays will characterize the MEK1-Cu complex and gain better insight on the Cu-interaction residues' roles within MEK1 (Tier 2) for phosphorylating ERK2 (Tier 3) when Cu (additive) is bound and unbound.

Materials and Methods

General Consideration

MaxQ™ 8000 Incubated Stackable Shakers (ThermoFisher Scientific): All of the protein growths for purification were conducted within the MaxQ™ 8000 Incubated Stackable Shakers (ThermoFisher Scientific). These stackable shakers have the durability to run at a top speed of 400 rpm overnight, contain a HEPA filter that ensures pure air inside the chamber and reduces cross contamination between protein growths, and a slide out platform that provides 100% sample access at all times.

ÄKTA pure 25 L and UNICORN software (GE Healthcare Life Sciences): All Sepharose and Superdex columns for protein purification were run on the ÄKTA pure 25 L (GE Healthcare Life Sciences) for Fast Protein Liquid Chromatography (FPLC). These instruments are used to further enhance affinity column protein purifications and separation from undesired products through a broad selection of hardware options (ie. valves, tubing, and columns). The UNICORN control software is also used to determine the protein elution and provides various readings, such as UV and mAmps, to further optimize protein purification techniques for each unique protein.

Beamline 24ID-C (Advanced Photon Source synchrotron): All crystals were shot at the Advanced Photon Source (APS) synchrotron through remote access for crystallographic studies. The APS synchotron is optimized to address cases in macromolecular crystallography by providing extremely stable and intense X-ray beams with beam sizes ranging from 5 to 70 microns. The 24ID-C beamline was solely utilized due to it being a variable energy beamline, which allowed for the energy of the beam to be tuned appropriately to detect the most electrons present for a specific element. This created an anomalous signal density that was present when solving the structures. This anomalous density was only present when the element of interest was bound to the structure. No anomalous signal would be detected unless the element of interest was present in the structure or crystal.

Invitrogen XCell II Blot Module and Novex XCell *SureLock* Mini-Cell (ThermoFisher Scientific): All SDS-Page gels transfers to PVDF membrane were conducted by an Invitrogen XCell II Blot Module in a Novex XCell *SureLock* Mini-Cell (ThermoFisher Scientific). This allows for easy transfer of proteins or nucleic acids from gels to membranes. It fits within the XCell *SureLock* Mini-Cell and requires less than 200 mL of

transfer buffer for Western, Southern, and northern transfers. Tough platinized titanium and stainless steel electrodes help create a uniform electrical field without clamps or hinged gel holders that are known to alter results.

EnVision Multilabel Plate Reader (PerkinElmer): All Enzyme-Linked ImmunoSorbent Assays were processed and read by the EnVision Multilabel Plate Reader (PerkinElmer). EnVision's wide range of filters and optical mirror modules cover the UV/Vis wavelength range, so direct measurement of DNA and protein is possible. This can also achieve high performance detection of all ELISA assays and immunoassays using different labels.

ImageJ Western Blot Quantification Software: Quantification of all Western bands were completed using the ImageJ software. This was completed by selecting an area by drawing a rectangle around the band. The same rectangular area was utilized for all the bands in each gel for each subset, ie. with or without DTT. A quantification number is displayed under or below each associated band.

Plasmids and Constructs

Multiple recombinant protein constructs were prepared for the experiments conducted in this study. Rabbit cDNA encoding a library of MEK1 residues from 1 – 393 was utilized for insertion into a PET28A vector with a N-terminal 6-Histidine-tag and cleavable TEV site (Met-Glu-Asn-Leu-Tyr-Phe-Gln-Gly-Ser) for tag removal. The PET28A plasmid is used as the vector to make the MEK1 protein and insert expressible in *E. coli* through the *lac* operon. PCR reactions were setup with the MEK cDNA library (insert) and the PET28A plasmid (vector), to excise the insert and create an opening in the vector for the insert. Similarly, MEK1 with an N-terminal GST-tag was inserted into a pGex-3t vector. These PCR reactions mixes occurred in two separate tubes and included 43 µL insert or 42 µL template (vector only), 1 µL restriction enzyme #1, 1 µL restriction enzyme #2, and 10 µL 10x Cut Smart buffer. To the reaction with vector alone, 1 µL of Calf Intestinal Phosphatase (CIP) was added to protect the cut ends of the vector from auto-ligating with itself. After the PCR reactions are complete, the insert:vector ratios of 0:2, 0.75:2, 1:2, and 1.25:2 were mixed and diluted up to 10 µL with nanopure water. A volume of 10 µL ligation mix was added to ligate the mixtures and allowed to incubate for 1 hour at 25°C on the bench. PCR on the insert only, then combine the plasmid and insert to ligate with the ligase. After PCR, 1 µL Dpn1was added to remove any methylated DNA nucleotide sites and incubated overnight. These ligation mixtures were added as 10 µL volumes into XL1Blue or DH5α cells to transform for DNA expression. After 20 minutes on ice, the samples were heat shocked at 42°C for 50 seconds and 250 µL of Lysogeny Broth (LB) was added to the cells. The cells shook at 37°C for 1 hour and were then plated on antibiotic agar plates. These were incubated overnight at 37°C for cell colony growth. Kanamycin at 1 mM was used for all 6-His-tagged constructs and 1 mM Ampicillin was used for GST-tagged constructs.

If colonies grew, they were mini-prepped by selecting colonies and placing each in a culture tube with 5 mL LB and 5 µL of antibiotic. These were shaken overnight at 37°C for growth. Next, the culture tubes were spun down for 15 minutes at 4200 rpm.

The solution was decanted, with the remaining pellet dissolved in 250 μL P1 resuspension buffer and transferred to an Eppendorf tube. The cells were then lysed with 250 μL P2 lysis buffer and inverted a few times to mix. Finally, 350 μL N3 neutralizing buffer was added to neutralize the cell lysis. The samples were then spun down at 13,300 rpm at 25°C for 10 minutes and the supernatant was decanted from the pelleted precipitate and applied to a spin column with a DNA binding membrane over a vacuum manifold. The supernatant was vacuumed off and a wash with 500 μL phosphate buffer (PB) to allow efficient binding of the DNA to the spin column. A final wash was carried out with 750 μL PE wash buffer to remove other unwanted components, while keeping DNA bound to the spin column. The spin column was spun for 1 minute at 25°C at 13,300 rpm to remove excess liquid in the spin column and another spin cycle with 30 μL of nanopure water was completed to elute the DNA off the spin column. These samples were then sequenced to confirm successful insertion by adding 3 μL of plasmid, 3 μL of forward/reverse primer, and 3 μL of nanopure water.

The following is a list of all the constructs produced for this study:

- 6-His-TEV constructs
  - MEK Full Length (FL)
    - Wild Type (wt)
    - H188A
    - H188F
    - C207S
    - H188A/C207S (double mutant)
  - MEK FL S218D, S222D (DD)
    - wt
    - H188A
    - C207S
    - Double mutant
- Glutathione-S-Transferase (GST) constructs
  - MEK1 FL
    - wt
    - H188A
    - C207S
    - C121S
    - Double mutant
  - MEK1 FL DD
    - wt
    - H188A
    - C207S
  - ERK2 FL
    - K54R
- Crystal constructs
  - MEK1 45 – 393 with a GSGSGS or SVQSDI linker region 6-His-TEV
  - MEK1 Δ62 – 393 with SVQSDI linker 6-His-TEV

.

Cloning and Mutagenesis

Cloning and mutagenesis of all constructs were carried out similarly with differences being in the primer concentrations and PCR reaction programs. The primers for site-specific mutagenesis were designed by mutating the nucleotide sequence of target codon for desired amino acid, with 21 nucleotide (equaling 7 amino acids) overhangs on 5' and 3' sides. The PCR reaction mixtures for mutagenesis contained 23 μL nanopure water, 1 μL of ~75 μg/μL template (plasmid), 0.5 μL 1:17 forward primer, 0.5 μL 1:17 reverse primer, 25 μL Master Mix; while cloning mixtures contained 23 μL nanopure water, 1 μL template (plasmid), 0.5 μL 1:100 forward primer, 0.5 μL 1:100 reverse primer, 25 μL Master Mix. After PCR, 1 μL Dpn1 was added to remove any methylated DNA nucleotide sites and incubated overnight. These were then transformed into DNA expression cell lines, ie. DH5α or BL21 (Gold) cells, through the addition of 10 μL PCR reaction to cells and placing on ice for 20 minutes. The samples were then heat shocked at 42°C for 50 seconds and 250 μL LB was added to cells and incubated for 1 hour at 37°C while shaking. These were then plated on antibiotic agar plates and incubated overnight at 37°C. DNA was extracted through the mini-prep protocol explained previously and sequenced to confirm protein sequence and mutations made.

Protein Expression and Purification

The DNA-sequenced constructs were transformed into protein expressing cell lines, ie. DE3 or Rosetta cells, for induction and expression in E. coli. A volume of 1 μL of plasmids were transfected into cells and incubated on ice for 20 minutes. The cells were then heat shocked at 42°C for 50 seconds and 250 μL LB was added. These samples were then incubated for 1 hour at 37°C shaking and then added to a 100 mL LB solution with 100 μL of 1 mM antibiotic. The inoculated LB solutions were shaken overnight at 37°C. A volume of 8 mL of the overnight growth and 1 mL of 50 mg/mL KAN for His constructs, or 100 mg/mL AMP, for GST constructs, were added to 1 L LB or TB.

His-tagged MEK1 proteins were expressed in Rosetta bacterial expression cells in E. coli at 37°C in MaxQ™ 8000 Incubated Stackable Shakers (ThermoFisher Scientific). These were induced with 1 mM IPTG after an OD of 600 was reached and left shaking overnight at 18°C. The next day, they growth were spun down and lysed through sonication in lysis buffer 25 mM Tris pH 8.0, 250 mM NaCl, 1 mM PMSF, and ~50 mg DNase. The lysate was then spun down at 18,000 rpm for 30 minutes, and the supernatant was added to 8 mL of equilibrated nickel (Ni-NTA) affinity resin. The supernatant was left to incubate and rotate at 4°C for 1 hr. The affinity column was then washed with 25 mM Tris pH 8.0, 250 mM NaCl, and 20 mM Imidazole. The MEK1-His-tag protein was eluted with 25 mM Tris pH 8.0, 250 mM NaCl, and 300 mM Imidazole. TEV was added to the protein to cleave between the N-terminus 6 His-tag and the beginning of the MEK1 sequence. This was occurred during overnight dialysis into a low salt buffer (25 mM Tris pH 8.0, 20 mM NaCl, and 5 mM BME) to run on a 5 mL Q-Sepharose anion exchange column. The one exception to this was the MEK 45 – 393 6-His TEV w/ SVQSDI or GSGSGS linker crystallization construct that was run over a 5 mL SP-Sepharose cation exchange column. The column with the 6-His-tag cleaved protein was run over a gradient of 20 mM – 1 M NaCl with 25 mM Tris pH 8.0 and 5 mM BME present. The peak fractions containing protein were run on an SDS-PAGE acrylamide gel to identify

peak protein fractions at the correct molecular weight (kDa). These fractions were combined and concentrated to ~12 mL to run over another Ni-NTA affinity resin column for a reverse Ni^{2+} to remove any remaining uncleaved His-tagged protein. This column was equilibrated, washed, and eluted with a 25 mM Tris pH 8.0, 250 mM NaCl, and 20 mM Imidazole buffer. The protein was then concentrated to run on a Superdex S200 gel filtration column in a final buffer of 25 mM Tris pH 8.0, 250 mM NaCl, 5 mM BME, and 5% glycerol. Protein was flash frozen in liquid nitrogen and stored in -80°C freezer for future use.

GST-tagged MEK1 and ERK2 K54R proteins were expressed in Rosetta bacterial expression cells for E. coli at 37°C in MaxQ™ 8000 Incubated Stackable Shakers (ThermoFisher Scientific). These were induced with 1 mM IPTG after an OD of 600 was reached and left shaking overnight at 18°C. The next day, they growth were spun down and lysed through sonication in lysis buffer 25 mM Tris pH 7.5, 250 mM NaCl, 1 mM PMSF, and ~50 mg DNase. The lysate was then spun down at 18,000 rpm for 30 minutes, and the supernatant was added to 8 mL of equilibrated Glutathione affinity resin. The supernatant was left to incubate and rotate at 4 °C for 1 hr. The affinity column was then washed with 25 mM Tris pH 7.5, 500 mM NaCl, and 5 mM BME. The GST-tagged protein was eluted with 25 mM Tris pH 7.5, 500 mM NaCl, and 20 mM glutathione buffer that was re-pH to 7.5 after addition of L-reduced Glutathione. The protein was dialyzed overnight into a low salt buffer (25 mM Tris pH 7.5, 20 mM NaCl, and 5 mM BME). After dialysis, the GST-tagged protein was concentrated and run on a Superdex S200 gel filtration column in a final buffer of 25 mM Tris pH 7.5, 250 mM NaCl, 5 mM BME, and 5% glycerol. If additional purification was needed, the dialyzed protein could first be run on a Q-Sepharose anion exchange column over a 20 mM – 1 M NaCl gradient. Lastly, protein was flash frozen in liquid nitrogen and stored in -80°C freezer for future use.

Crystallization

MEK1 45 – 393 w/ SVQSDI linker at 10 mg/mL was mixed with 2 mM Adenylyl-imidodiphosphate (AMP-PNP) w/ and w/o 2 mM Mg^{2+}. Trays were setup with the crystal condition of varying polyethylene glycol (PEG) 3350 concentrations (8 - 24%), 4% Glycerol, 200 mM NH_4F, 10 mM dithiothereitol (DTT) (99% pure, cat #BP172-25, Fisher BioReagents) using the hanging-drop vapor diffusion method at 4°C. Cu was soaked in by soaking in solution without DTT present and by doing long, short, and back soaks in various concentrations of Cu^{2+}. Cryo-conditions were obtained by taking the mother liquor and increasing the glycerol to 20%. Crystals obtained were used for X-ray diffraction data collection at the Advanced Photon Source synchrotron (beamline 24ID-C). This tunable beamline was used to shoot at an anomalous edge of ~9.1 keV in order to detect anomalous density corresponding to the position of Cu in the structure. The crystals of MEK1 45 – 393 with SVQSDI linker with and without Cu were processed using HKL-2000.

All of the crystal structures were determined by molecular replacement in PHENIX using Phaser. The apo MEK1 45 – 393 with SVQSDI linker structure was determined using PDB 3SLS[9] as a search model in Phaser, which was then used for the MEK1 45 – 393 Cu-bound structures as a search model. Model building and refinement were performed with Coot and PHENIX. AMP-PNP was built into the structure by

downloading its PDB file and building it in through PHENIX and then running the structure through PHENIX refine. Table 1 statistics were produced using the PHENIX validation tools. Cu binding coordinates were drawn in by Coot based on the displayed density within the structure. This electron density was confirmed to not be Mg^{2+} due to the absence of Mg^{2+} in these crystal conditions and the beamline's tuned wavelength detecting solely Cu density. The Cu-coordination sites of H188, C207, and D208, match residues that were previously tested through mutational studies *in vivo*.[3]

In vitro studies

Western Immunoblotting

Protein samples were prepared to a total volume of 26 μL with concentrations of 200 nM MEK1 FL, 25 nM MEK1 DD FL, or 1 μM MEK1 FL wt GST (crude); 4.5 μM ERK2-GST K54R; 5 – 20 μM Cu(I), Cu^{2+}, or Ag^{+}; and 100 μM ATP. MEK1 and ERK2 were diluted with kinase buffer (50 mM HEPES pH 7.0, 50 mM NaCl, and w/ & w/o 2 mM DTT), while ATP was diluted with ATP dilution buffer (10 mM $MgCl_2$, 50 mM HEPES pH 7.0, and 200 mM NaCl). The reactions were shaken for 5 minutes and then left standing on the bench for 35 minutes at 25°C. The reactions were quenched with 5x loading dye and boiled at 95°C for 5 minutes. The samples were then run and separated on 12.5% sodium dodecyl sulfate polyacrylamide gels. Proteins were transferred onto a nitrocellulose membrane (cat #170−4152, Bio-Rad) using a Trans-blot Turbo transfer system (Bio-Rad). Nitrocellulose membranes were blocked in 2.5% Nonfat milk in TBS containing 1% Tween-20 (TBST) for 45 minutes at 25°C. Incubation with primary antibody of phospho- Erk1/2 (T202/Y204) rabbit antibody (for cell signaling) at 1:1000 dilution was performed overnight at 4°C in 2.5% Nonfat milk in TBST. Membrane was washed four times (5 minutes each time) with TBST and followed by a 1 hour incubation with Alexa Fluor-labeled secondary antibody (goat-anti rabbit IgG (H+L)-HRP conjugate, cat #170-66515, Bio-Rad)) at a 1:5000 dilution in 2.5% Nonfat milk in TBST. Immunocomplexes were visualized after secondary antibody by washing the membrane four times (5 minutes each time) with TBST and developing with 5 mL of Pierce SuperSignal ECL solutions 1 and 2 together for 5 minutes. The excess ECL was shaken off the nitrocellulose membrane and was then wrapped in plastic wrap to be placed in a autoradiography development cassette (FBXC 810, FisherBiotech) with BIOMAX MR chemiluminescent film within a photography dark room. The film was developed with a film development machine.

Enzyme-Linked IimmunoSorbent Assay (ELISA)

Protein samples were prepared at concentrations of 200 nM MEK1 FL or 25 nM MEK1 DD FL; 2.4 μg/μL ERK-GST K54R; 5 – 20 μM Cu(I), Cu^{2+}, or Ag^{+}; and 100 μM ATP. MEK1 and ERK2 were diluted with kinase buffer (50 mM HEPES pH 7.0, 50 mM NaCl, and w/ & w/o 2 mM DTT), while ATP was diluted with ATP dilution buffer (10 mM $MgCl_2$, 50 mM HEPES pH 7.0, and 200 mM NaCl). All volumes stated should be interpreted as volume per well. A glutathione-coated 96-well plate (Pierce, cat#15240) was initially washed with 200 μL TBST to remove impurities and equilibrate the wells for 15 minutes. TBST wash was decanted and 100 μL of ERK2-GST K54R as added to each well with a multi-channel pipette. The mixture was sealed and shaken for 1 hour at 25°C. ERK-GST K54R was decanted and was mixed with 200 μL of 1X TBST for 15

minutes. In a plastic 96 well tray, 100 μL of protein (untagged MEK) was aliquoted into each well and mixed with 1 μL additional additives (Cu, Ag, etc.) to allow thorough mixing and even incubation times. From the aliquoted protein-additive mixes, 50 μL was added to the well and then 50 μL of 200 μM ATP was added to the glutathione plate. The mixture was sealed and shaken for 5 minutes, then incubated at 25°C for 40 minutes. The protein-reaction mixture was decanted and 200 μL of 1X TBST was added to the wash and shaken for 15 minutes. The primary antibody of phospho-Erk1/2 (T202/Y204) rabbit antibody (for cell signaling) (cat #9101, Cell Signaling Technology) was diluted to 1:5000 into a dilution solution of 0.25% Bovine Serum Albumin (BSA) in 1X TBST. 100 μL of primary antibody was added and shaken for 1 hour. The primary antibody solution was decanted and washed twice by adding 200 μL of 1X TBST and shaken for 15 minutes twice. After both washes, 100 μL of Alexa Fluor-labeled secondary antibody (goat-anti rabbit IgG (H+L)-HRP conjugate, cat #170-66515, Bio-Rad) was added at a 1:5000 dilution in 0.25% BSA in 1X TBST solution and shaken for 1 hour. The secondary antibody solution was decanted and washed three times with 200 μL of 1X TBST for 10 minutes each time. After decanting washes, 5 mL of each SuperSignal ELISA Pico Chemiluminescent Substrate (Pierce #37069) solutions were mixed and add 100 μL of the mixture was added to the plate. The plate was read on a PerkinElmer EnVision. Each value was repeated in duplicate or triplicate and averaged. The error bars are the calculated standard errors for each triplicate.

Mass Spectrometry

An acrylamide gel electrophoresis was run with the samples of interest. The gel was handled with gloves on to prevent potential contaminants and followed the same procedure for staining and developing the protein bands as a normal gel with the excess Coomasie stain was removed by soaking in destain solution of 20% methanol, 10% glacial acetic acid, and 70% nanopore water. These were then sent for LC-MS/MS for the bands of interest and the control band for the comparison with other bands. The bands of interest were cut out, digested with trypsin, and the digests were analyzed by LC-MS/MS on a Q-Exactive Plus mass spectrometer. The mass spec data were searched against the combined UniProt E. coli/Sf9 database plus the recombinant protein sequence you have provided using the MaxQuant 1.5.2.8 program. False discovery rates for protein and peptide identifications are set at 1%. This showed all of the identified proteins. Common contaminants (e.g. keratins) were removed, and proteins were required to have a minimum of 2 nonredundant (razor+unique) peptides. Different Intensity levels and MS/MS count columns were recorded to see which proteins were more abundant in each sample. This produced reports for the protein of interest and provided a summary of the analysis.

Results and Discussion

Crystal structure of the MEK1-Cu complex and implications for Cu regulation of MEK1

To understand the molecular basis for the interaction between MEK1 and Cu, a crystal structure of MEK1 with and without Cu bound was determined. For crystallographic studies of MEK1 without Cu, MEK1 45 – 393 His TEV with a SVQSDI or GSGSGS linker was utilized. The 6-residue linkers replaced residues 264 – 307, which included a flexible loop that makes MEK1 difficult to crystalize. The condition

that produced the highest resolution crystals contained 18% PEG 3350, 4% glycerol, 10 mM DTT, 200 mM NH_4F, and 2 mM AMP-PNP with and without Mg^{2+} (Figure 4). After crystals were formed, soaks were conducted to remove DTT from the condition and soak in metals for efficient metal binding. For the apo MEK1 45 – 393 crystals, the space group was P1 2_1 2 with 2 MEK1 molecules in the asymmetric unit and the 3SLS structure was a search model for molecular replacement. The phased molecular replacement structure produced a data set of 2.3 Å resolution with solid geometry and refinement statistics (Table 1). The search model (3SLS) and solved apo-structure were consistent with each other. Both structures had different space groups of $P2_1$ and P1 2_1 2 and the solved apo-MEK1 structure had 2 MEK1 subunits within the asymmetric unit (Figure 5a). The observed MEK1 dimer in the asymmetric unit appears to be an artifact of crystal packing due to there being no residue contacts for MEK1 dimerization to occur. The active state of kinases with an Asp-Phe-Gly (DFG) motif is determined by either the position of the entire loop being flipped in (active)[10] or out (inactive)[10], or the Asp or Phe positions within the active site[10]. The overlaid structures (Figure 5b, 5c) show similarities in their active sites, with both DFG loops in the DFG-out conformation. The solved apo-MEK1 45 – 393 structure's Asp was flipped out and the Phe flipped in (Figure 5b, 5c), both of which signal an inactive conformation. apo-MEK1 structure also did not contain Mg^{2+} and the ATP-binding site was occupied by ADP. This is interesting, due to the apo-soaking condition containing $MgCl_2$ and there being a prominent metal binding site that this study is probing. While the lack of Mg^{2+} within the apo-structure differed from the search model, this could be beneficial for future metal binding soaks. Due to Mg^{2+} absence, the potential issue of metal binding affinity for metal displacement, ie. Mg^{2+} for Cu^{2+}, should not be an issue. Another observation made was the density within the active site only contained space for 2 phosphate groups at the ATP binding site, thus ADP was modeled. The ADP present in the structure may be one reason that an inactive conformation was observed. This would have been formed due to the used ligand, AMP-PNP, which is an ATP analogue with a non-hydrolyzable phosphate bond. Since the kinase could simulate the ATP hydrolysis reaction with the AMP-PNP, it is possible that this locked the MEK1 F209 in an inactive or "off" conformation. These absences are the most probable cause for the major difference between the 3SLS and the apo-MEK1's Asp208 side chains positioning being significantly different. In the apo-MEK1 structure, the Asp208 is flipped away from the search model's Asp208 (Figure 5c). This was likely caused by the α-helix proceeding the DFG-motif being closer to the active site due to the absence of Mg^{2+} and ATP's third phosphate group. These absences would allow for the α-helix slight flexibility within the active site confines to coil sooner and move closer to the DFG-motif.

Upon solving the MEK1 structure without Cu, various attempts were made to introduce Cu to the protein for X-ray structure determination. This was done by optimizing the condition to 20% PEG 3350, 4% glycerol, 200 mM NH_4F, 2 mM AMP-PNP. Cu was introduced in a crystallographic setting through long, quick, or back soaks of Cu^{2+} at varying concentrations. These crystals were used for X-ray data collection using a tunable beamline at an anomalous signal of ~9.1 keV in order to confirm and ensure the presence of Cu (Figure 6a). Electron density differences were observed after analyzing the crystallography data with molecular replacement, PHENIX, and Coot, while utilizing the solved apo MEK1 45 – 393 structure as the search model for the

molecular replacement. These differences included a large density cloud within the active site region (Figure 6b), which appears to be sharing density with the C207 side chain.

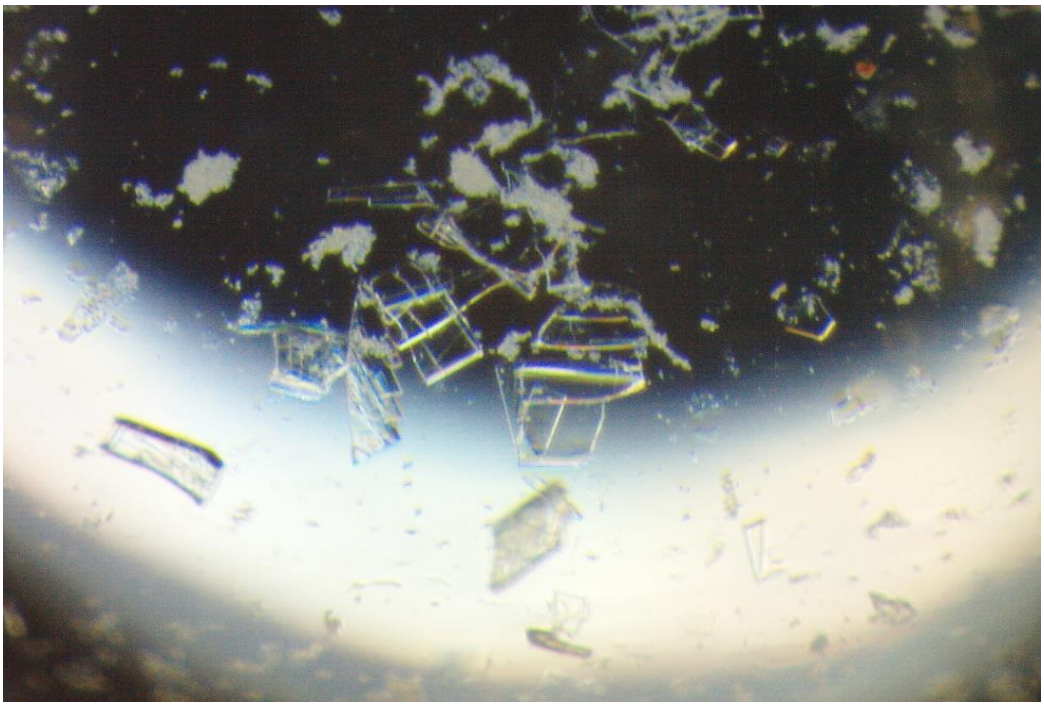

Figure 4. MEK1 45 – 393 w/ SVQSDI linker apo crystals. These are rectangular in shape and have a tendency of forming off of one another or plating back-to-back. These apo-crystals are looped to remove DTT and used to soak in the metal of interest.

The interaction sites were detected with the cysteine and histidine residues' side chains, C207 and H188 respectively (Figure 6a). The observation of Cu^{2+} at this site is not unusual, since this is also the site for Mg^{2+} and is directly upstream of the DFG-motif that binds to ATP. Like Mg^{2+}, we believed that Cu^{2+} had bound here due to it being a regulatory site. The C207 residue is the closest ligand and appears to have the largest effect on the Cu based on the shared density displayed during refinement, while the H188 side chain and D208 backbone help coordinate the Cu, and the F209 flips inward to cap the Cu in place. Interaction distances are drawn (Figure 6c) in order to clarify the coordinating sites, due to only 1 site (C207) having a confirmed interaction with the Cu through density sharing. The distances drawn from the Cu had values of 2.1 Å (H188) 2.3 Å (C207), and 2.3 Å & 2.0 Å (D208's backbone carbonyl and amide groups). While F209 appears to cap the Cu, its bond distance (~10 Å) is too great to have any direct effect on the Cu. Given all of the drawn distances (Figure 6c), these residues (H188, C207, and D208's backbone) were determined to have van der Waals interaction forces responsible for coordinating the Cu ion. Other studies that have studied Cu sites by crystallography[11,12] have observed common trends of geometry patterns with Cu. Given the distances for this structure, there were two potential geometry organizations for this Cu, disordered tetrahedral or square planar coordination. The disordered tetrahedral geometry typically has drastically unsymmetrical distances for each bond length and is associated to Cu^{+}.[11,12] The MEK1-Cu structure's H188 and C207 bond lengths, as noted

above, are approximately equivalent. This equivalence or symmetry is a characteristic associated solely with the square planar conformation.[12] The square planar conformation is associated to Cu^{2+} and generally observed for inactive state proteins.[12] This helped to conclude that the Cu oxidation was Cu^{2+} with the solved MEK1-Cu structure and the inactive state was further confirmed by the DFG residues' positions. To see how drastic of a conformational change the Cu^{2+} caused the apo structure was overlayed with the Cu bound structure (Figure 7). The most notable difference is the change that D208 undergoes, which shifts out of the way to allow the Cu^{2+} to "bind". Another large structural change is the H188 side chain flipping inward toward the Cu^{2+} to help coordinate it in place. This residue (H188) has another notable feature of being part of the HRD domain. The His-Arg-Asp (HRD) domain is a regulatory motif within the catalytic loop that helps regulate the kinase activity of MEK1 by properly positioning the DFG-Asp and αC-helix's Lys-Glu contacts.[13] While the HRD domain does not directly cause phosphorylation, it is an important regulatory site that when affected, drastically influences the activity level of MEK1. Finally, C207 and F209 shift accordingly to enhance the interaction of the other residues with Cu.

Table 1. Summary of MEK1 Crystallographic Statistics.

Crystal	MEK1 45 - 393 wt His-cut w/ SVQSDI (w/o Cu)*	MEK1 45 - 393 wt His-cut w/ SVQSDI (w/ Cu)*
Resolution range (Å)	50 - 2.4 (2.44 - 2.4)	50 - 2.3 (2.34 - 2.3)
Space group	P1 2_1 1	P1 2_1 1
Unit cell ***(a, b, c, α, β, γ)***	46.581, 94.739, 72.793, 90, 93.28, 90	47.042, 95.027, 72.288, 90, 94.2, 90
Total reflections	51133	88824
Unique reflections	22800	26017
Redundancy	2.2 (2.2)	3.3 (2.8)
Completeness (%)	92.71 (88.24)	90.94 (65.42)
Mean ***I/σ(I)***	9.50 (4.71)	7.98 (2.70)
Wilson B-factor	24.43	28.65
R-merge	0.063 (0.142)	0.11 (0.752)
R-work	0.1957 (0.2151)	0.2528 (0.3473)
R-free	0.2495 (0.2781)	0.3020 (0.4153)
Number of atoms	4813	4552
macromolecules	4518	4552
ligands	62	
water	201	0
Protein residues	598	598
RMS (bonds)	0.004	0.003
RMS (angles)	0.81	0.82
Ramachandran favored (%)	98	98
Ramachandran outliers (%)	0	0
Clashscore	6.29	5.86
Average B-factor	30.9	45.6
macromolecules	30.8	45.6
ligands	31.9	
solvent	32.6	

*PHENIX refined statistics produced from solved MEK1 45 – 393 wt His cut w/ SVQSDI linker with and without Cu bound structures.

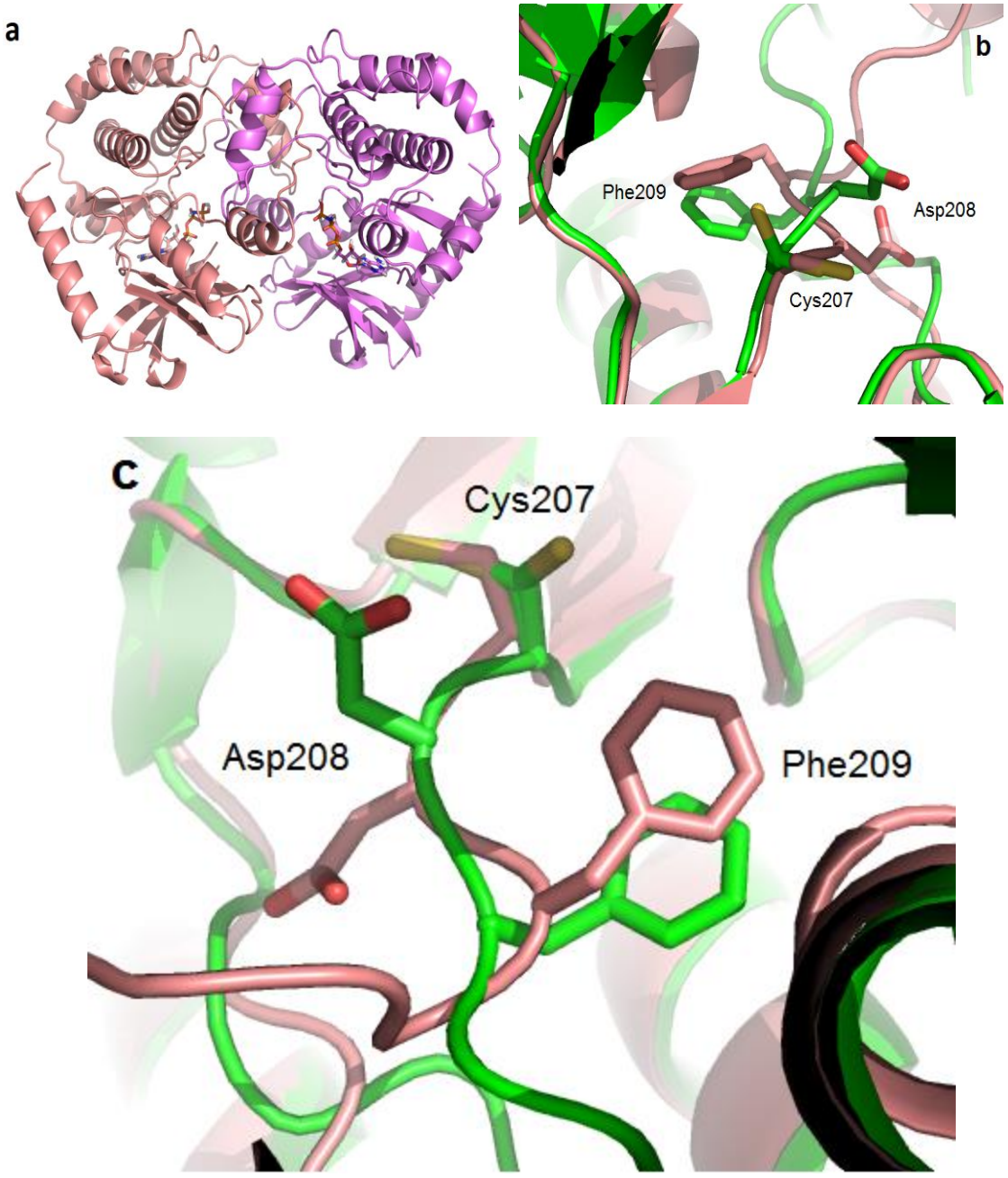

Figure 5. MEK1 45 – 393 w/ SVQSDI linker apo structures: (a) the crystal packed MEK1 dimer with ADP bound and absence of Mg^{2+}, (b) vertical perspective of active site with search model 3SLS (green) and apo-MEK1 structure (pink) overlaid displaying Phe209 and Cys207 with little vertical differences, while Asp208 occupy very different spots on the vertical plane, (c) horizontal view of active site with search model 3SLS and apo-MEK1 structure overlaid showing Phe209 and Cys207 with minimal differences, while the apo-MEK1 structure's Asp208 is flipped away from the search model's Asp208 position.

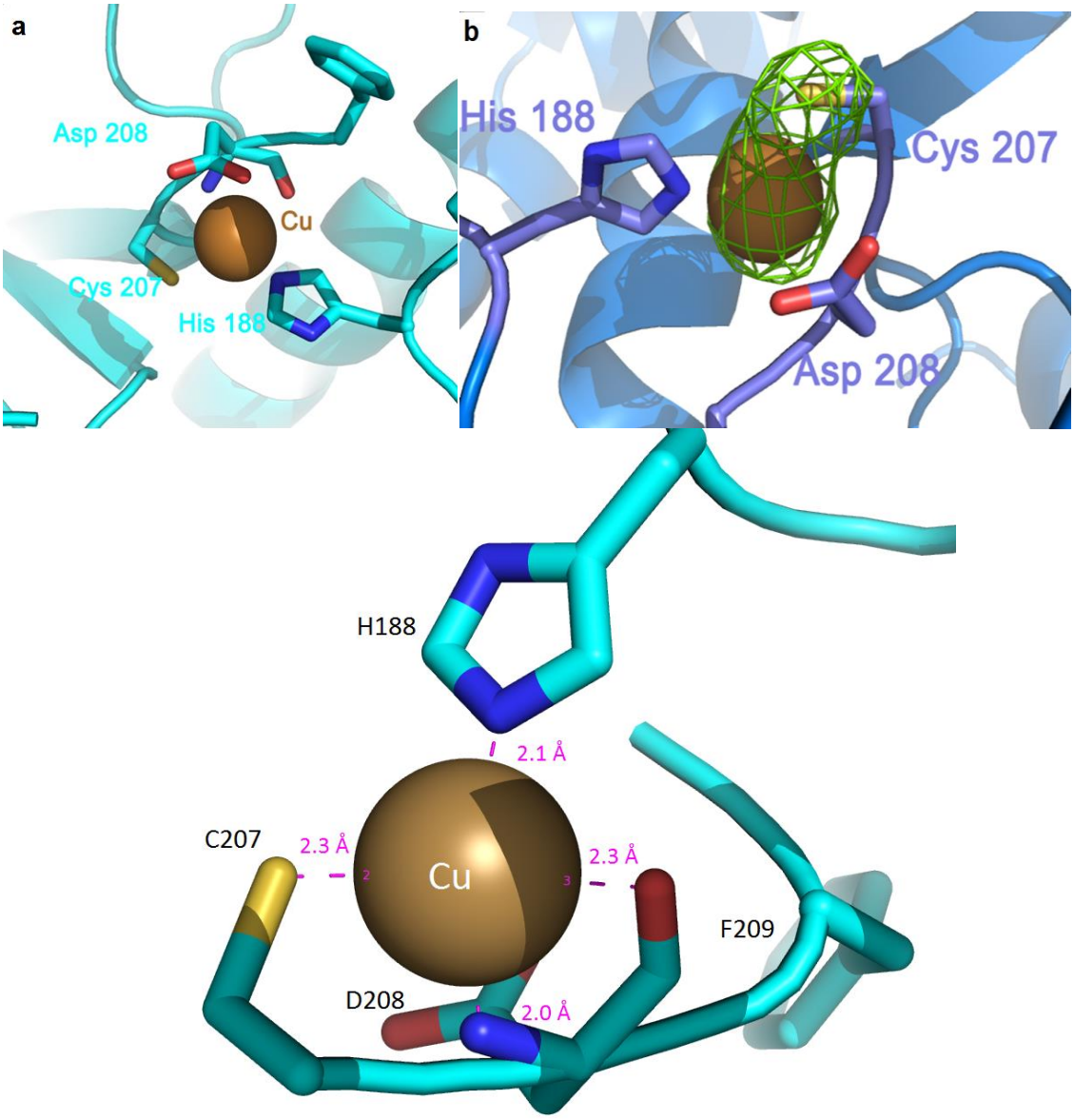

Figure 6. MEK1 45 – 393 w/ SVQSDI linker with Cu^{2+} bound in the active site: (a) labeled residues interacting and coordinating the Cu^{2+} atom, (b) the density cloud with a Cu^{2+} atom built in after refinement. The Cu^{2+} density cloud appears to be sharing space with C207, which could indicate a bond forming or simply a strong coordination residue, (c) the Cu^{2+}'s drawn coordinating sites and distances to determine the coordination geometry of Cu^{2+} and the coordinating residues. Given the distances and residue positions square planar was the determined Cu^{2+} coordination geometry.

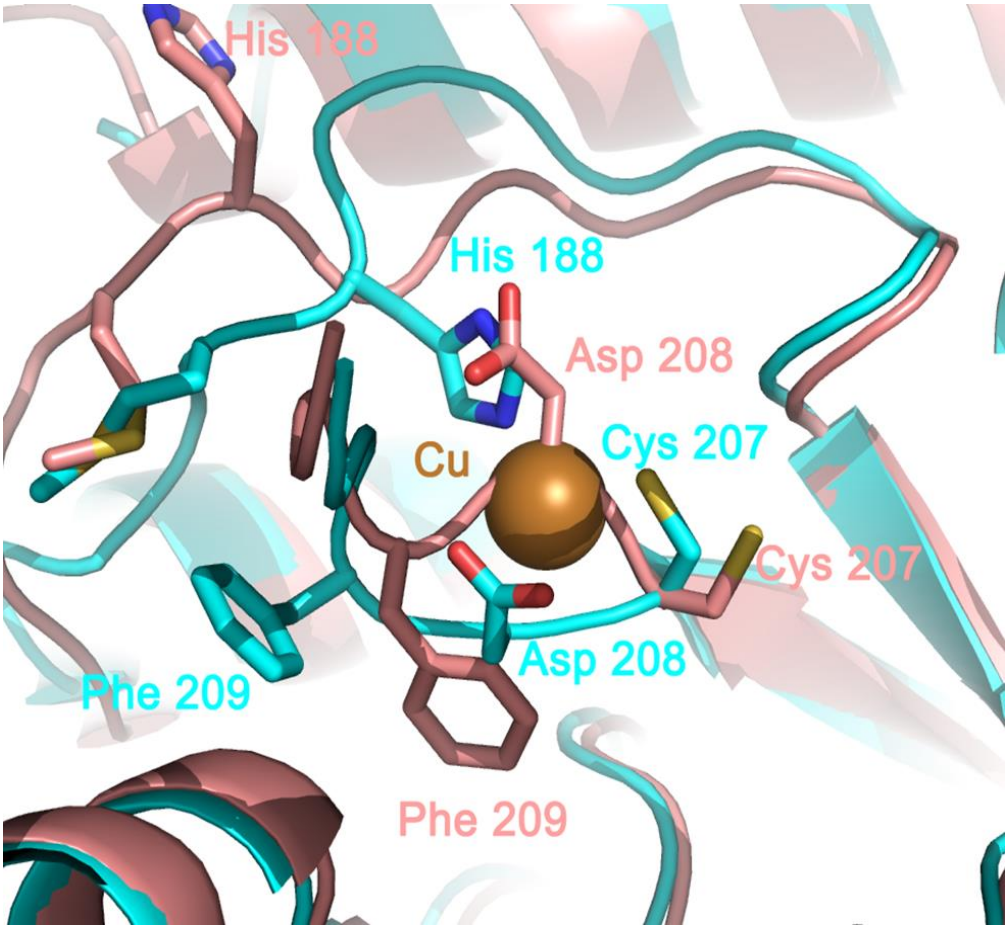

Figure 7. Overlay of MEK1 45 – 393 w/ SVQSDI apo (pink) and Cu-bound (cyan) structures. Distinct change of H188 flipping towards the active site to coordinate the Cu atom. Asp208 side chain and backbone both move back to coordinate the Cu atom as well. The Cys207 side chain moves closer to the Cu atom, which correlates to the shared density observed when solving the structure (Figure 5b). Phe209 shifts outward to cap the Cu atom, which potentially helps strengthen the other coordinating interactions.

In vitro Studies of Copper Regulation of MEK1

To functionally characterize the importance of the Cu ligands observed in the crystal structure, mutagenesis studies targeted the H188 and C207 residues. While D208 does coordinate the Cu ion, it is also a part of the DFG-motif, which is responsible for contributing to kinase activity within the active site. Therefore, it was decided to not mutate D208 since it would be difficult to distinguish between effects on catalysis from Cu interaction. New constructs harboring mutated residues were prepared including: C207S, H188A, and a H188A/C207S double mutant. The wild-type and mutant constructs were qualitatively tested for activity using the western immunoblotting technique. The blot results clearly indicated a change in the kinase activity. Compared to wild type MEK1, MEK1- C207S showed reduced ERK2 phosphorylation while MEK1-H188A has no detectable activity (Figure 8). As mentioned previously, H188 is a part of the MEK1 HRD-motif. Depending on the kinase, the HRD-His or HRD-Asp residues are important because they mediate H-bonds to the Asp residue within the DFG-loop of the kinase, which mediates kinase activation.[14] The mechanistic importance of the HRD-His

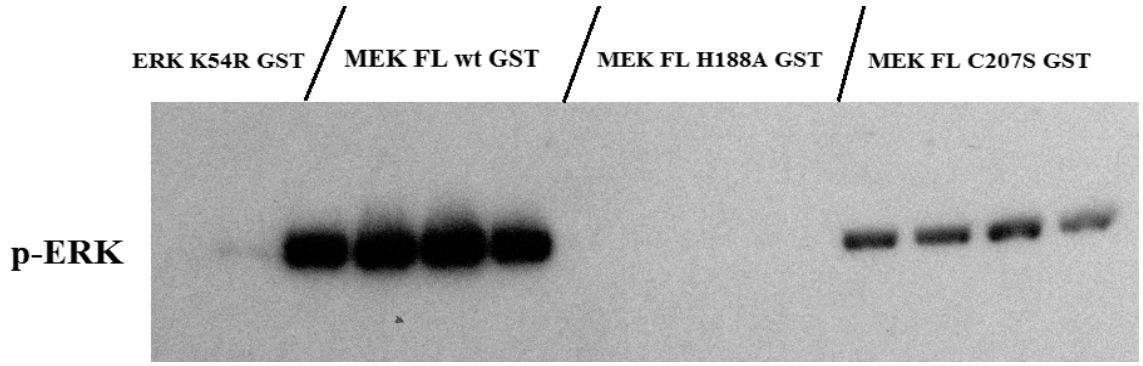

Figure 8. Initial Western blots of MEK1 Full Length (FL) wild type (wt), H188A, and C207S GST-tagged constructs. These were conducted show active protein was being produced during protein purification and could be used for additional kinase activity measurement assays.

position has not been studied, thus it is unknown how the HRD-His would affect kinase activity. Its mutation in other studies either causes a reduction (~30%) or elimination of activity dependent on the kinase studied.[13]

We then carried out a more quantitative enzyme-linked immunosorbent assay (ELISA), to assess MEK1 activity. The initial activity counts of p-ERK signal during the optimization of the ELISA was quite low, making it difficult to determine the effect of mutations on MEK1 activity. To overcome this, additional mutations were made in MEK1 at residues to mimic the phosphorylated active form of MEK1, S218D and S222D (MEK1-DD). We found that MEK1-DD was 46 times more active than MEK1-WT (Appendix 1). This phosphomimetic construct, MEK-DD, was utilized during the ELISA assay to reduce protein usage and increase activity counts to better observe changes caused by the mutations and Cu-addition. After testing various concentrations of Cu, inhibition was observed (Figure 9) instead of the activation observed in previous studies.[3] Slow incorporation of Cu through overnight dialysis was attempted, since this would allow the Cu to be added gradually to MEK1 and prevent the protein from crashing out of solution. Each of these was tested on a Western blot and ELISA for activity; however, no signal was detected. ELISA experiments were further conducted on MEK1-DD, MEK1-WT, and mutant constructs in the presence and absence of Cu. This lead to the conclusion that all solutions used killed the kinase during dialysis (Figure 10). Testing other variables, such as kinase buffers (Figure 11a), protein concentrations, and other metals, inhibition was the primary observation. When testing different reducing agents (Figure 11b) without additional additives, activation at various levels was observed. Even with the C207S mutant that has drastically reduced activity compared to wild type, inhibition was still consistently observed (Figure 12).

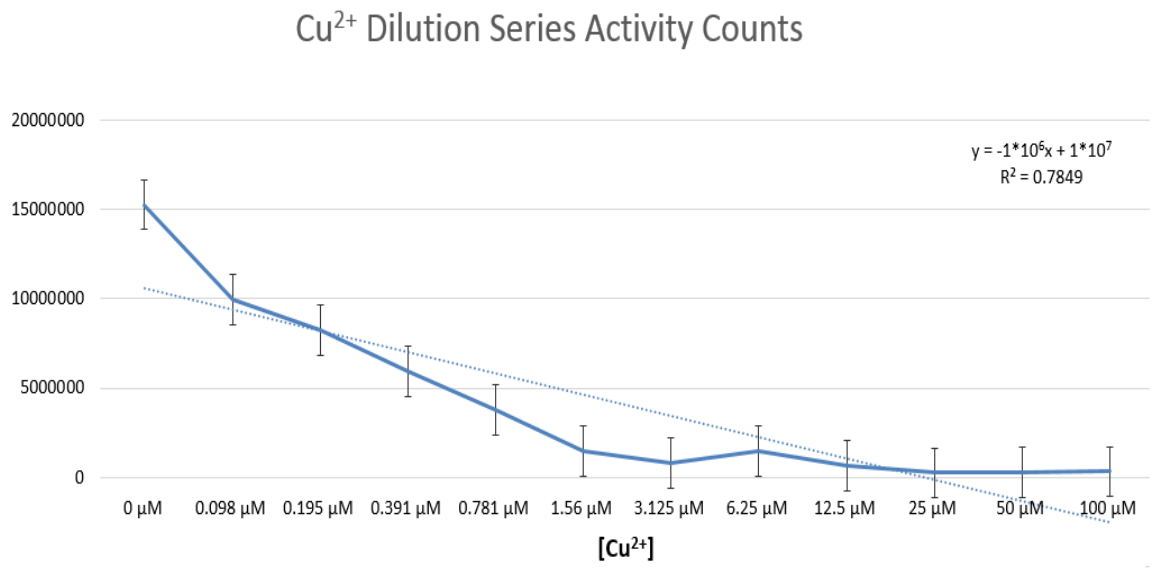

Figure 9. Varying Cu concentrations with 200 nM MEK1-6His cut FL wt and 4.5 µM ERK-GST K54R. This graph shows the activity counts (y-axis) with standard errors and a negative correlation, signaling inhibition.

To address the possibility that during growth or purification of MEK1, endogenously bound metals were binding to MEK1, and thus preventing Cu binding, the metal chelator ammonium tetrathiomolybdate (TTM) was added to a dialysis of MEK1 before the sizing column buffer change. This TTM-purified MEK1-WT and MEK1-DD was used in the ELISA assay with 1 mM DTT and varied Cu^{2+} concentrations from 39 nM – 10 µM. The ELISA data revealed that MEK1 wt and MEK1 DD are consistently inhibited by Cu even after purification with TTM (Figure 13 a,b). Finally, reducing agent dithiothreitol (DTT) was added to the kinase buffer to better simulate a cell's reducing environment. This would not only provide a better environment for the kinase, but effect any important elemental oxidation states. This was further investigated by keeping the DTT or Cu levels constant and varying Cu or DTT concentrations, respectively. We observed that adding DTT alone or in excess of Cu did show significant MEK1 activation, but the addition of Cu to DTT typically showed dose response MEK1 inhibition (Figure 14). This data collectively indicates that DTT activates bacterially produced recombinant homogeneously purified MEK1 while Cu reduces MEK1 activity, consistent with what is expected from the observed Cu binding site in the crystal structure.

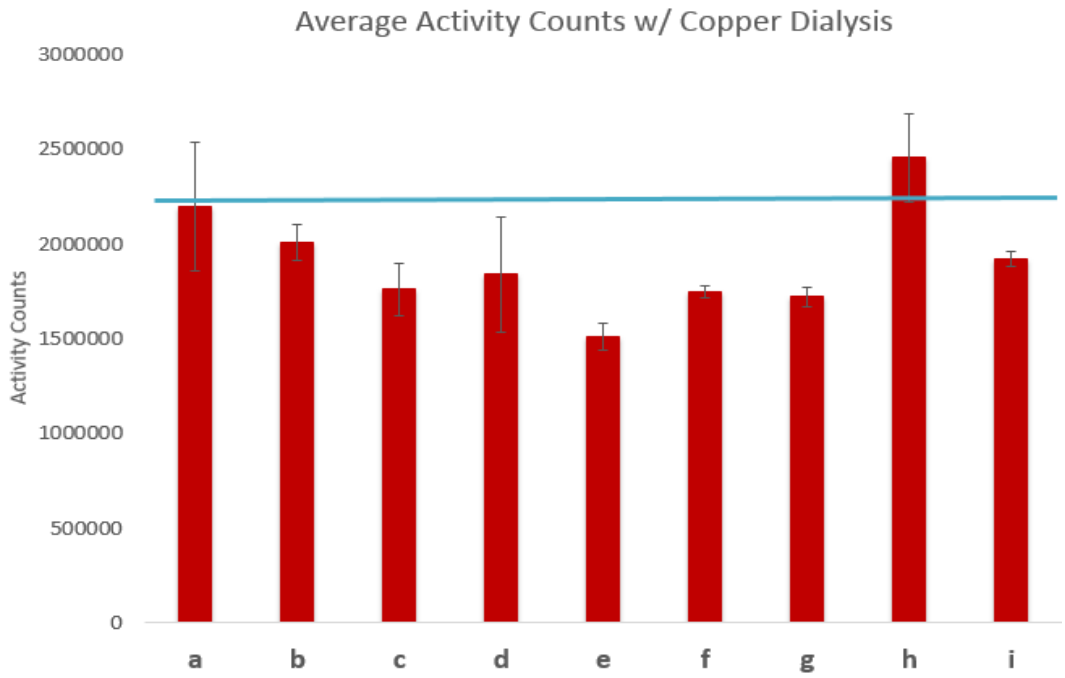

Figure 10. Various dialysis solutions used with 25 nM MEK1-6His cut FL DD and 200 nM MEK1-6His cut FL wt w/ TTM to slowly add Cu to the system. The solutions consist of the following: (a) 100 mM NaCl, 20 mM Tris pH 7.5, (b) 0 nM Cu^{2+}, 25 nM MEK1 DD wt, (c) 50 nM Cu^{2+}, 25 nM MEK1 DD wt, (d) 1 µM Cu^{2+}, 25 nM MEK1 DD wt, (e) 50 nM Cu^{2+}, 50 nM Imidazole, 25 nM MEK1 DD wt, (f) 1 µM Cu^{2+}, 1 µM Imidazole, 25 nM MEK1 DD wt, (g) 1 µM Cu^{2+}, 1 µM Imidazole, 200 nM MEK1 wt, (h) 1 µM Cu^{2+}, 1 µM Imidazole, 200 nM MEK1 wt w/ TTM, 2 µM Cu^{2+}, (i) 1 µM Imidazole, 25 nM MEK1 DD wt. The red line signals the baseline activity of MEK1 in the kinase buffer. All of the others were overnight dialysis with Cu, and are well below the red line, signaling that all of the MEK1 kinase in those solutions showed no activity. The one solution (g) with activity above the baseline was re-run and was dead upon re-testing.

Cu/Ag Displays Activation of Crudely Purified Recombinant MEK1

To better understand the DTT and Cu interaction, Western blots were revisited in order to use smaller amounts of protein and test more protein–additive reactions. Both MEK1-WT with either a 6His or GST tag, displayed inhibition with Cu^{2+} without DTT and baseline activity was surpassed upon DTT addition (Figure 15). While both GST and His constructs showed inhibition without DTT and no change with DTT present, there were differences observed with activity levels between the same constructs differing solely in their solubility tags. The MEK-GST tagged proteins tended to show stronger bands in lane 2 & 9, signaling more activity than the MEK1-His proteins in lane 5 & 12. Since endogenously bound metal is a possibility with a 6His-tag through either culture growth with media or interaction with Ni^{2+} on the resin, it was expected that metal was binding to the Cu-binding site through purification and introducing artifacts to the study. For these reasons, the GST-tagged constructs were used for further studies.

Oxidation state became a factor to consider, since DTT is required for activation and appears to be interacting and reducing the kinase or Cu^{2+} to allow for activation. For this reason, Cu^{+} and Ag^{+} were analyzed alongside with Cu^{2+}. Since Cu^{+} is extremely unstable and unfavorable, Tetrakis(acetonitrile) copper(I) hexafluorophosphate, abbreviated to Cu(I) for this study, was used to add Cu^{+} to the solution. Cu(I) is a

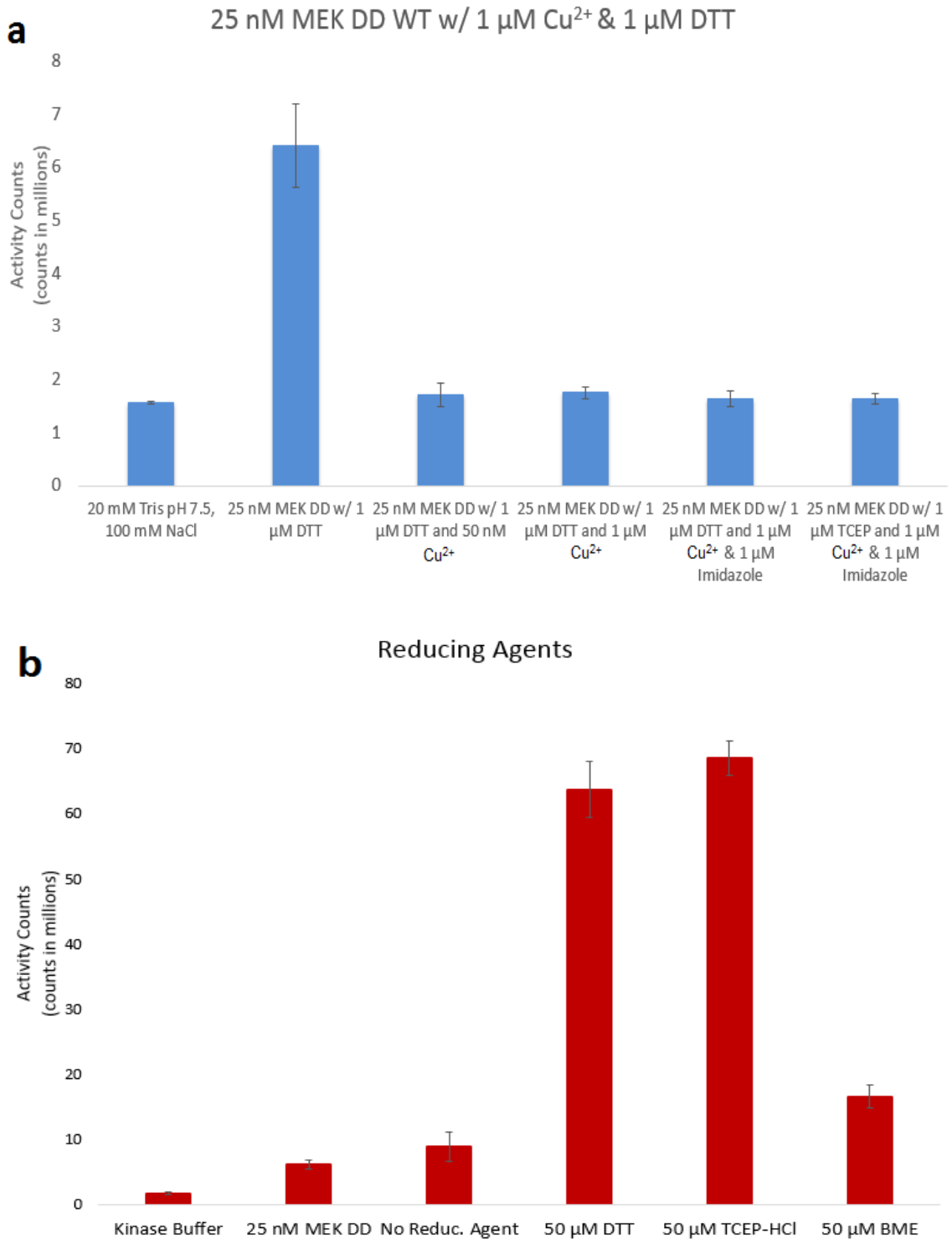

Figure 11. Other variables tested to characterize the Cu interaction with MEK1: (a) 25 nM MEK-6His cut FL DD undergoing dialysis with buffers varying reducing agents, imidazole concentrations, and Cu concentrations, where all dialysis solutions rendered the MEK1 kinase dead and (b) 25 nM MEK-6His cut FL DD with different reducing agents at the same concentration (50 µM) to see their effects on the kinase. All of the ones tested activated MEK1 to various degrees.

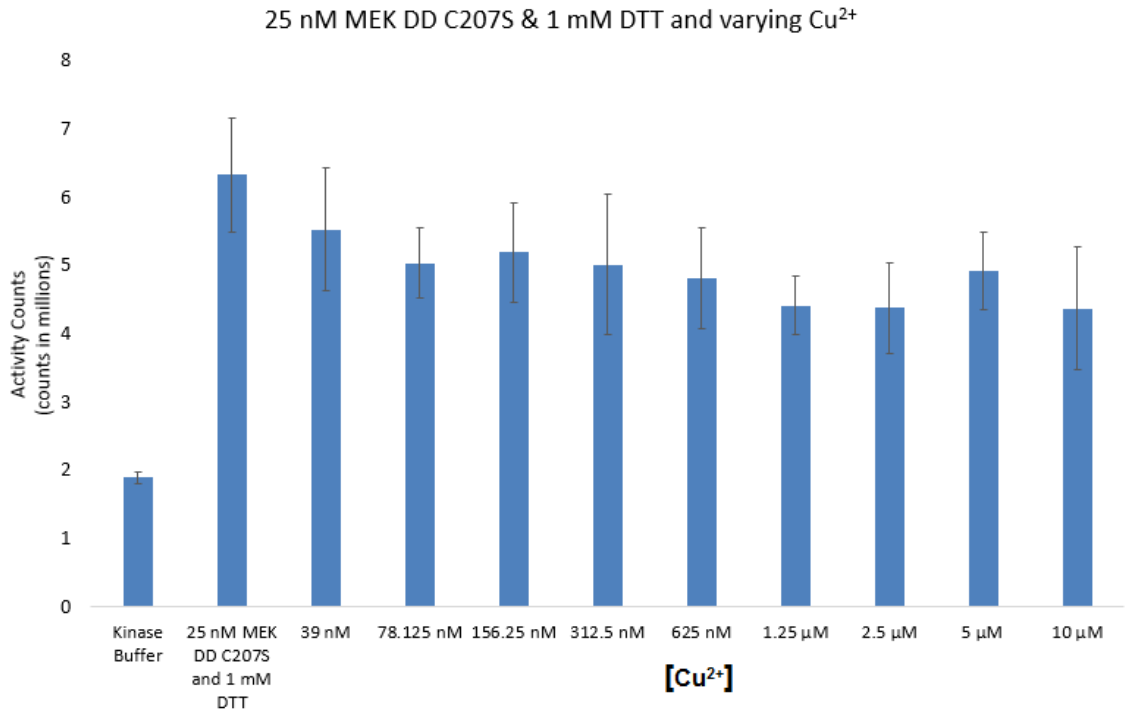

Figure 12. Testing C207S mutant with increasing Cu concentrations. 25 nM MEK-6His cut FL DD C207S to test increasing Cu concentrations' effects on a mutant construct, where Cu also killed the C207S's minimal activity levels with a constant 1 mM DTT present.

compound that stabilizes the Cu^{+} atom through multiple N-cyanide bonds and the PF_6^{-} allowing additional stabilization of the Cu^{+} compound.

MEK1 FL wt 6His-cut was tested first, due to its high purity and consistent purification results (Appendix 2). When run with Cu^{2+}, Cu(I), and Ag^{+}, Westerns displayed consistent inhibition at the few concentrations tested. In order to further probe the possibility of activation at a low concentration, serial dilutions for Cu(I) (Figure 16a) and Ag (Figure 16b) were conducted. The Cu(I) Western blot displayed correlated inhibition whereas the metal concentration increases, the activity level decreases without DTT in lanes 2-7 (Figure 16a). The Ag Western blot displayed possible activation without DTT present in lanes 4-6 that seem to have larger p-ERK bands than MEK1 wt without additives in lane 2 (Figure 16b). Additionally, there are some instances with DTT where Ag appear to inhibit in lanes 12-13 where the bands are smaller than the MEK1 wt without additives in lane 10 (Figure 16b).

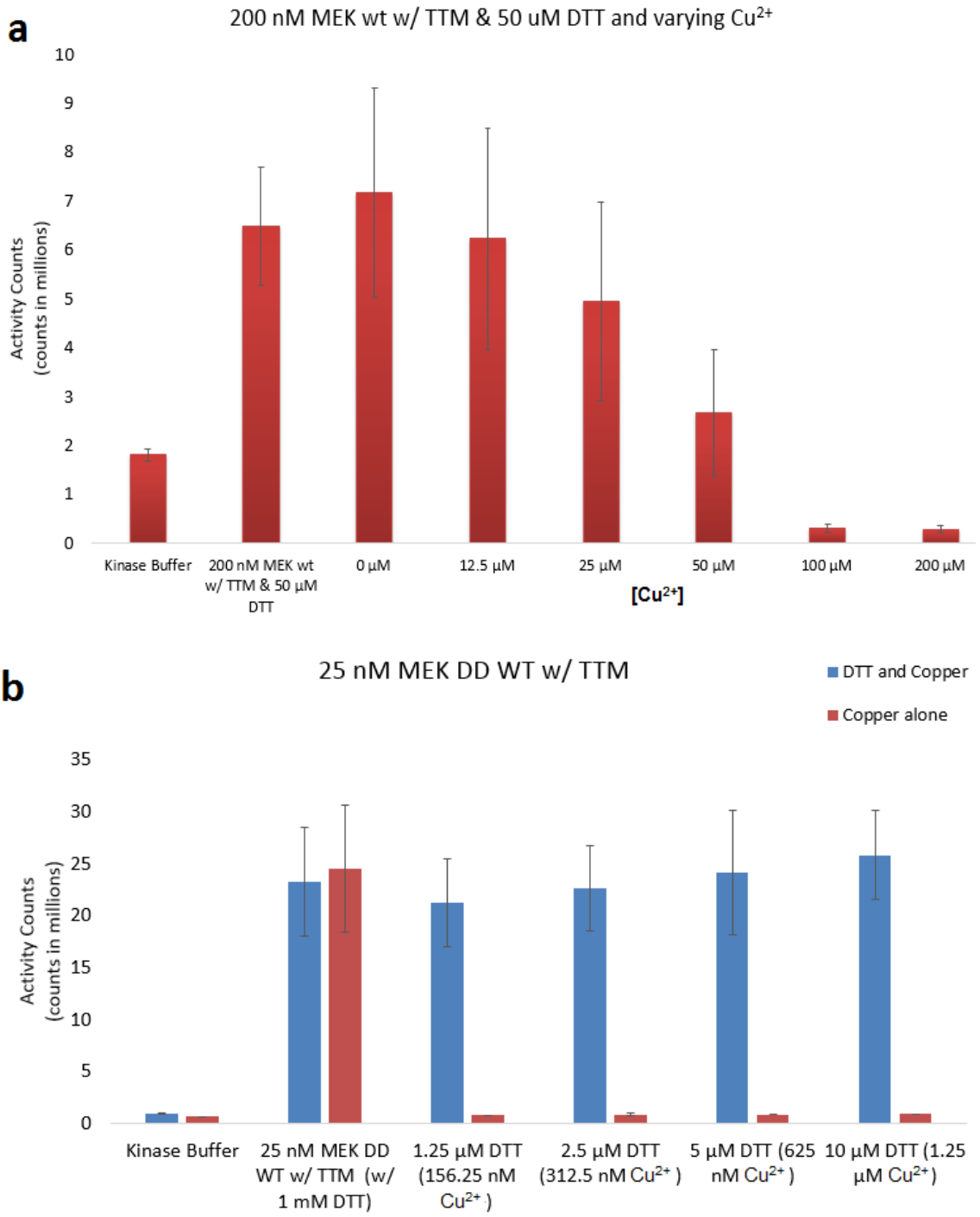

Figure 13. MEK1 purified w/ TTM and varying Cu concentrations: (a) 200 nM MEK-6His cut FL wt w/ TTM and DTT, showing inhibition as the Cu concentrations increase, specifically where the Cu:DTT concentration ratio is 1.25:1 or higher, (b) 25 nM MEK-6His cut FL DD with DTT and Cu which sees baseline activity, while Cu additions without DTT kill MEK1's activity.

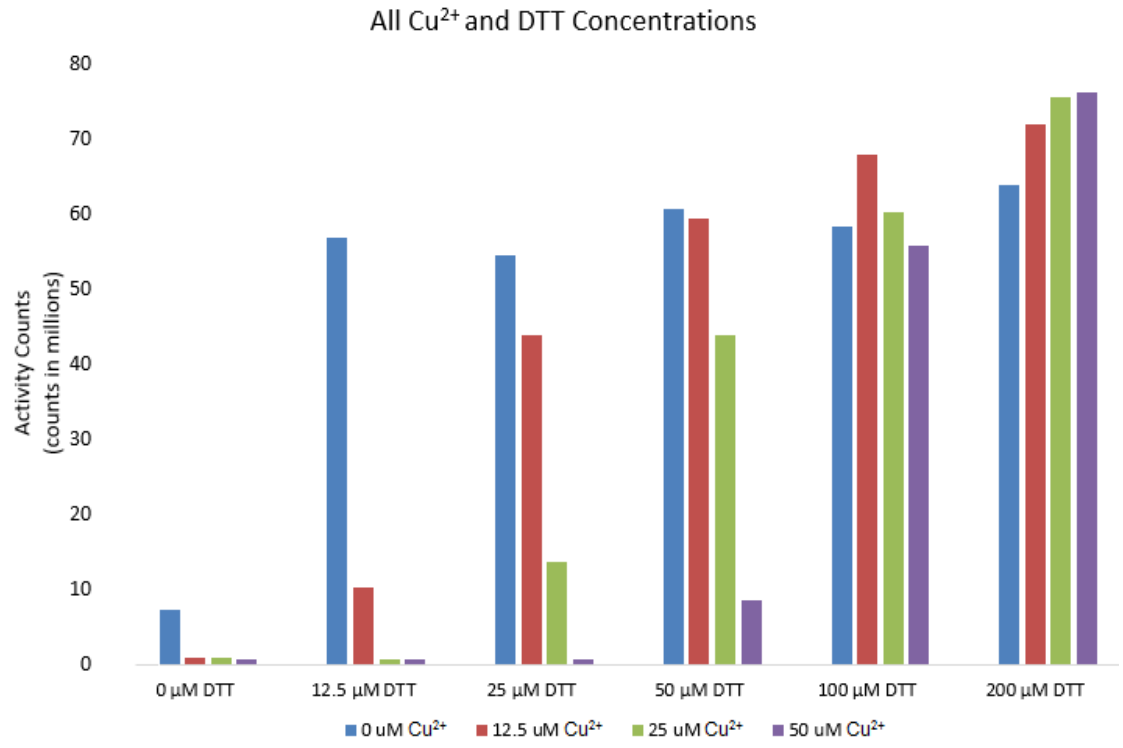

Figure 14. Varying Cu and DTT concentration ratios with 25 nM MEK-6His cut FL DD. The bottom values on the x-axis are the DTT concentrations present in that set of samples. Each color represents a different Cu concentration. There is a Cu:DTT concentration ratio that must occur in order for MEK1 to remain active and counteract the inhibitory effects of Cu.

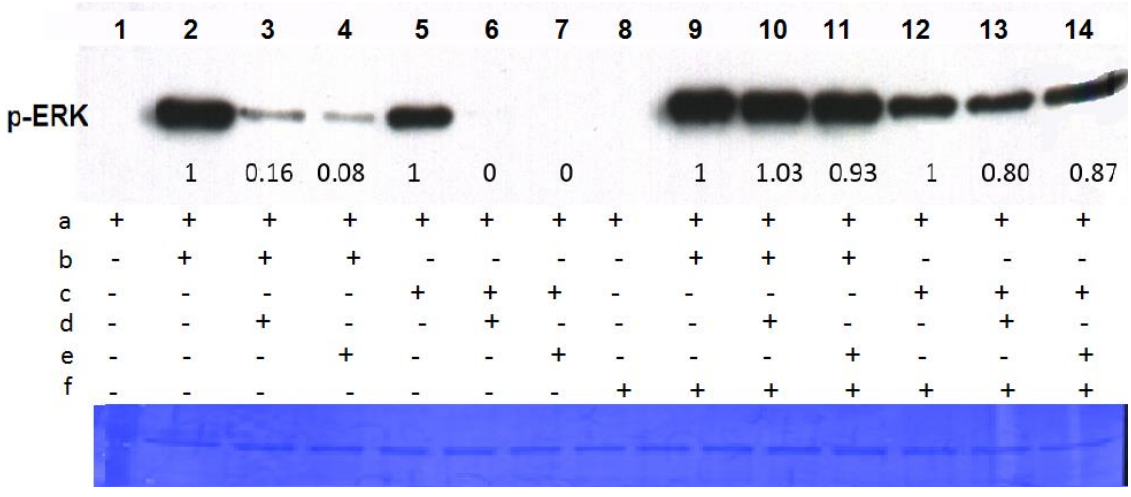

Figure 15. MEK1-wt purified with 6His- or GST-tag. The following species were present (+) or absent (-): (a) 4.5 µM ERK-GST K54R, (b) 200 nM MEK-GST FL wt, (c) 200 nM MEK-His cut FL wt, (d) 5 µM $CuSO_4$, (e) 10 µM $CuSO_4$, and (f) 2 mM DTT. Lanes 2-7 have an absence of DTT and show inhibition at two Cu concentrations, while lanes 9-14 have 2 mM DTT present and have the same activity levels as the samples with no Cu added. The Coomassie stained PVDF membrane blot below shows even loading amongst the lanes and confirms that the results are true.

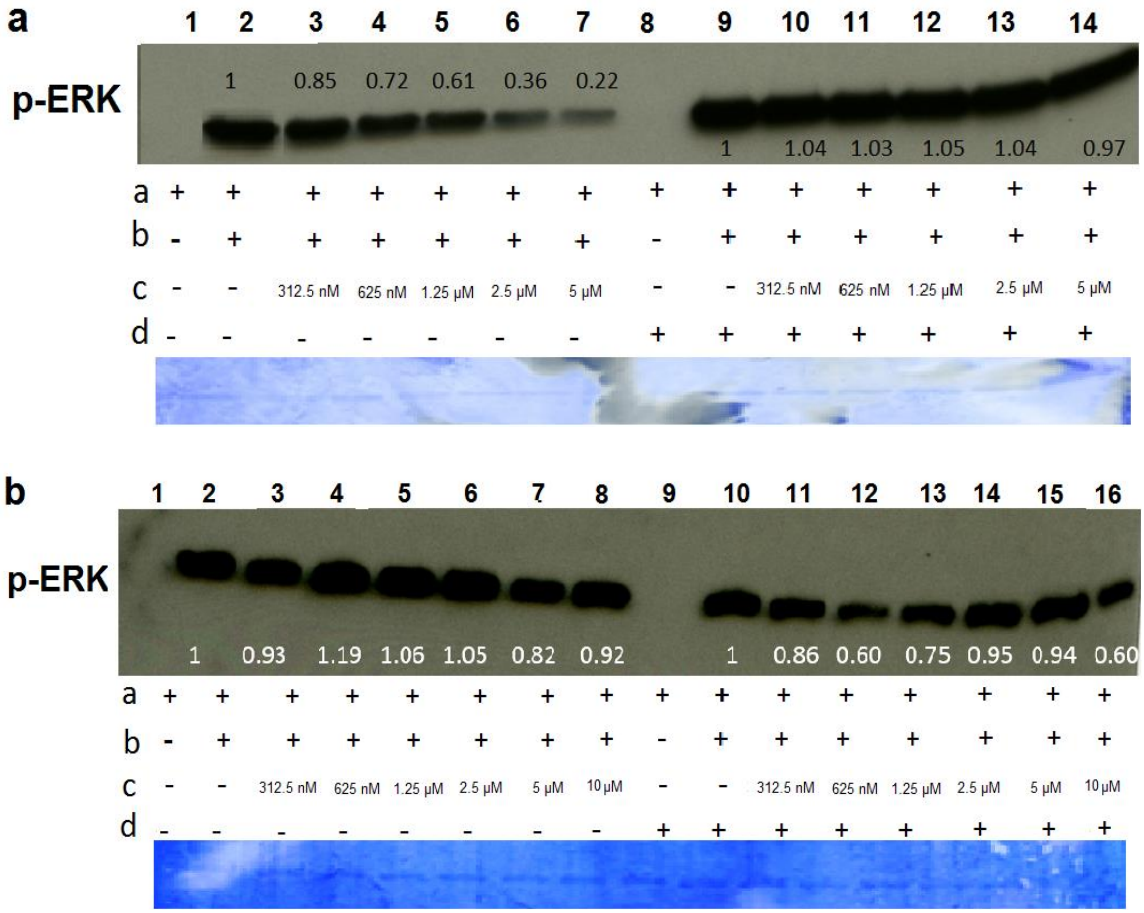

Figure 16. MEK1 FL wt 6His-cut metal analysis by Western blot of: (a) Cu(I) with **a:** 200 µg/ µL ERK-GST K54R, **b:** 200 nM MEK-6His cut FL wt, **c:** Cu(I), **d:** 2 mM DTT and (b) Ag with **a:** 200 µg/ µL ERK-GST K54R, **b:** 200 nM MEK-6His cut FL wt, **c:** Ag, **d:** 2 mM DTT. Inhibition is the clear trend for Cu(I), while Ag shows some possible activation without DTT present. Both have the Coomassie stained PVDF membrane blot below displaying even loading amongst the lanes and confirms that the results observed.

MEK1-GST FL wt was then prepared and concentrated after the dialysis step of purification. Some GST protein purifications do not include an S200 sizing run after eluting off of an affinity column due to their high specificity. The crude (unsized) MEK1-GST FL wt was determined by a gel electrophoresis (Figure 17a). Although the sample was clearly not pure, it was analyzed for MEK1 activity and Cu activation, due to this purification mimicking what was conducted by Brady et al. to demonstrate Cu activation.[3]

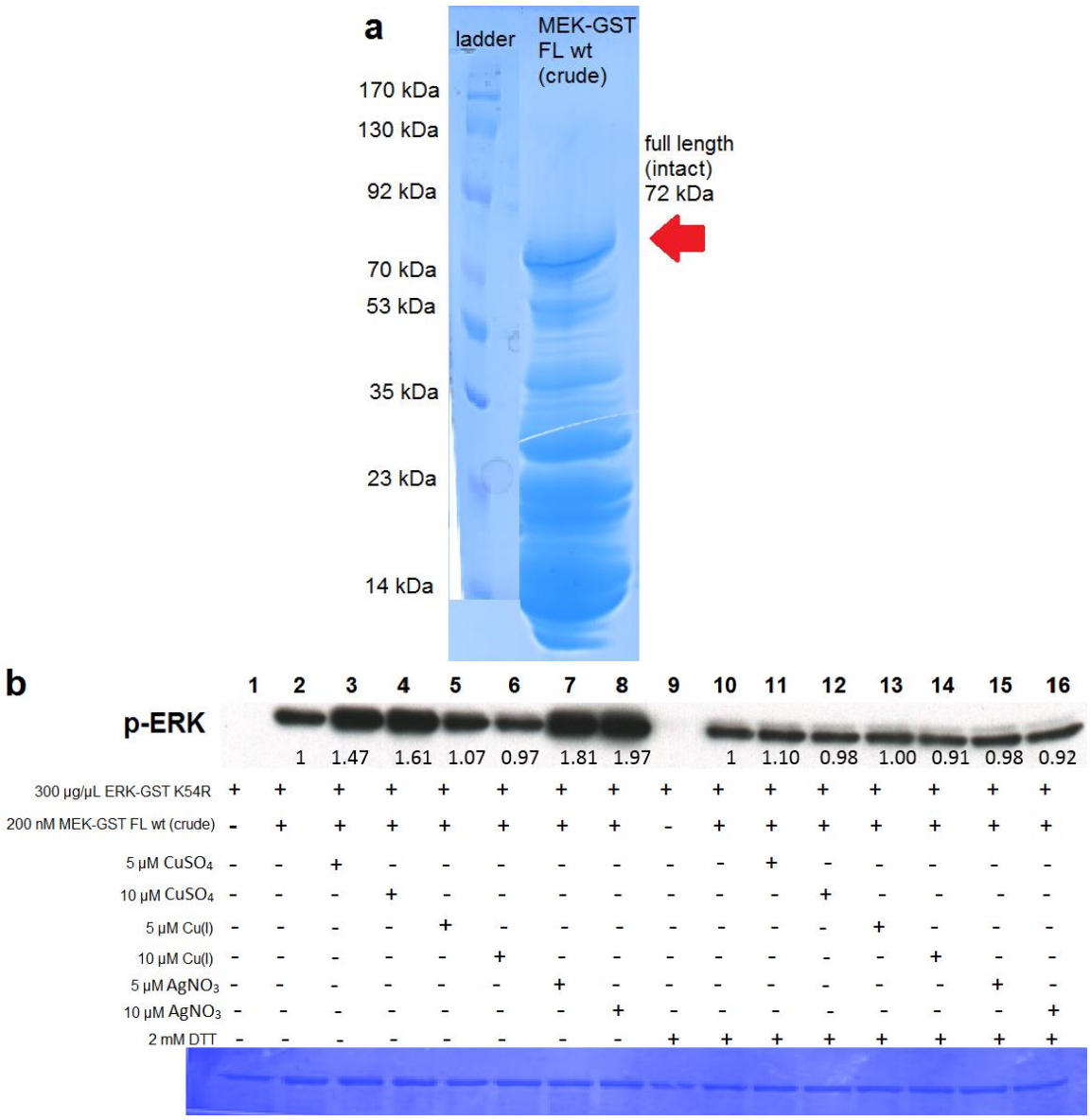

Figure 17. MEK1 FL wt GST crude sample analysis: (a) gel electrophoresis of MEK1 FL wt GST without S200 run and (b) Western blot of MEK1 FL wt GST crude concentrated sample with the following species present or absent. The Coomassie stained PVDF membrane blot below shows even loading amongst the lanes and confirms that the results are true.

The Western blot analysis demonstrated that the crudely purified MEK-GST FL wt was activated upon the addition of Cu^{2+}, Cu^{+}, and Ag^{+} without DTT present, while activity levels equal to MEK1 with no metal additives was achieved when DTT was present (Figure 17b). In order to identify what was causing the activation, a new GST-MEK1-WT sample was prepared and fractions from the glutathione resin were analyzed for kinase activity and metal activation using Western blot. This Western blot displayed four fractions with activity, each with its own interaction profile to the additives. Fraction #14 showed the strongest p-ERK signal, with Cu^{2+} activation without DTT present and Ag^{+} activation and Cu^{2+} inhibition with DTT present (Figure 18).

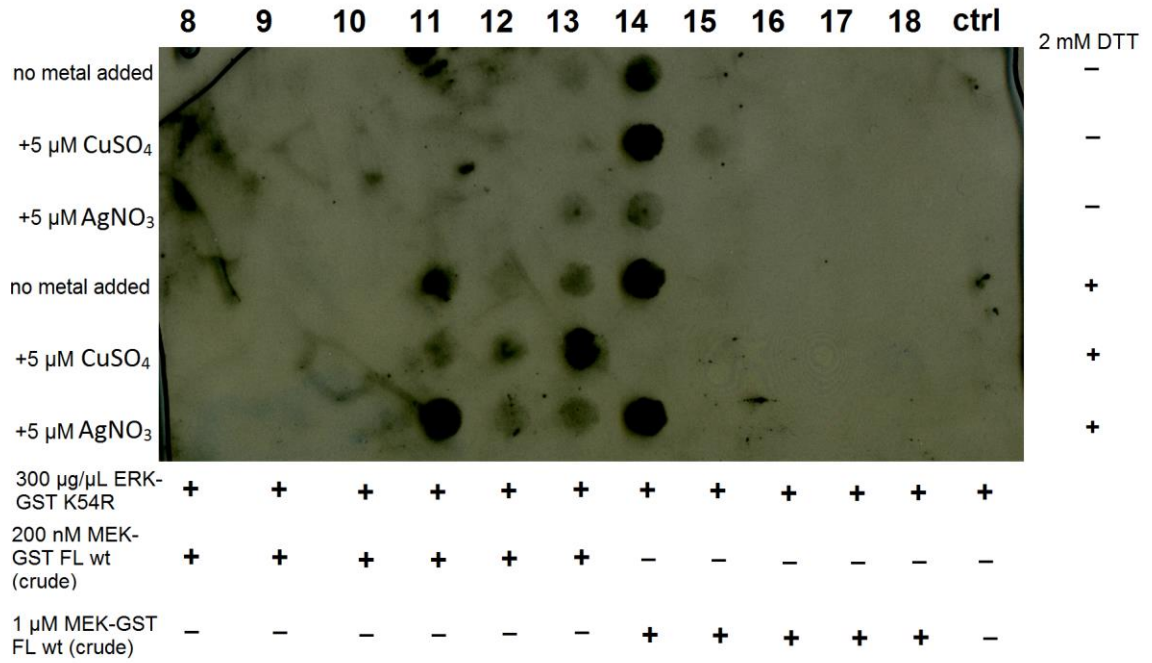

Figure 18. Western dot blot of MEK1 FL wt GST fractionated samples.

Fraction #14 was re-fractionated on an S200 sizing run and displayed strong lower bands (~40 kDa) that did not correlate to the MEK1-GST FL wt expected molecular weight band (72 kDa) (Figure 19a). The first three fractions of this gel displayed bands around 72 kDa and were combined and run on another Western (Figure 19b), which confirmed the dot blot results of activation apparent for Cu^{2+} and Cu^{+} without DTT present and slight activation with Ag^{+} with DTT present.

From these results, a gel with Fraction #14 was run and the strong lower bands, Band A and B (Figure 20) were sent for gel mass spectrometry to determine what is potentially causing the activation observed in crude MEK1-GST FL wt samples and reactions. These bands while more prominent within specific fractions, are present in all of the fractions and for this reason could be contributing to the observed activity levels regardless of its concentration within the specific fraction. Even at low concentrations, the degradation product's effect could be so strong that it is able to overcome the full length and other degradation product interactions occurring. The intact band was determined to be MEK1 –GST FL with no modifications and that Bands A and B contained mostly MEK1 proteins with few contaminants. Band was determined to be mostly comprised of N-terminus to K402 and Band B was composed of N-terminus to K330. The GST sequence that is part of this construct runs from residues 1-250, thus these residues had to be subtracted to determine exactly which residues of MEK1 were within the degradation bands. After the subtraction, Band A was comprised of MEK1 residues 1-152 and Band B was comprised of MEK1 residues 1-80.

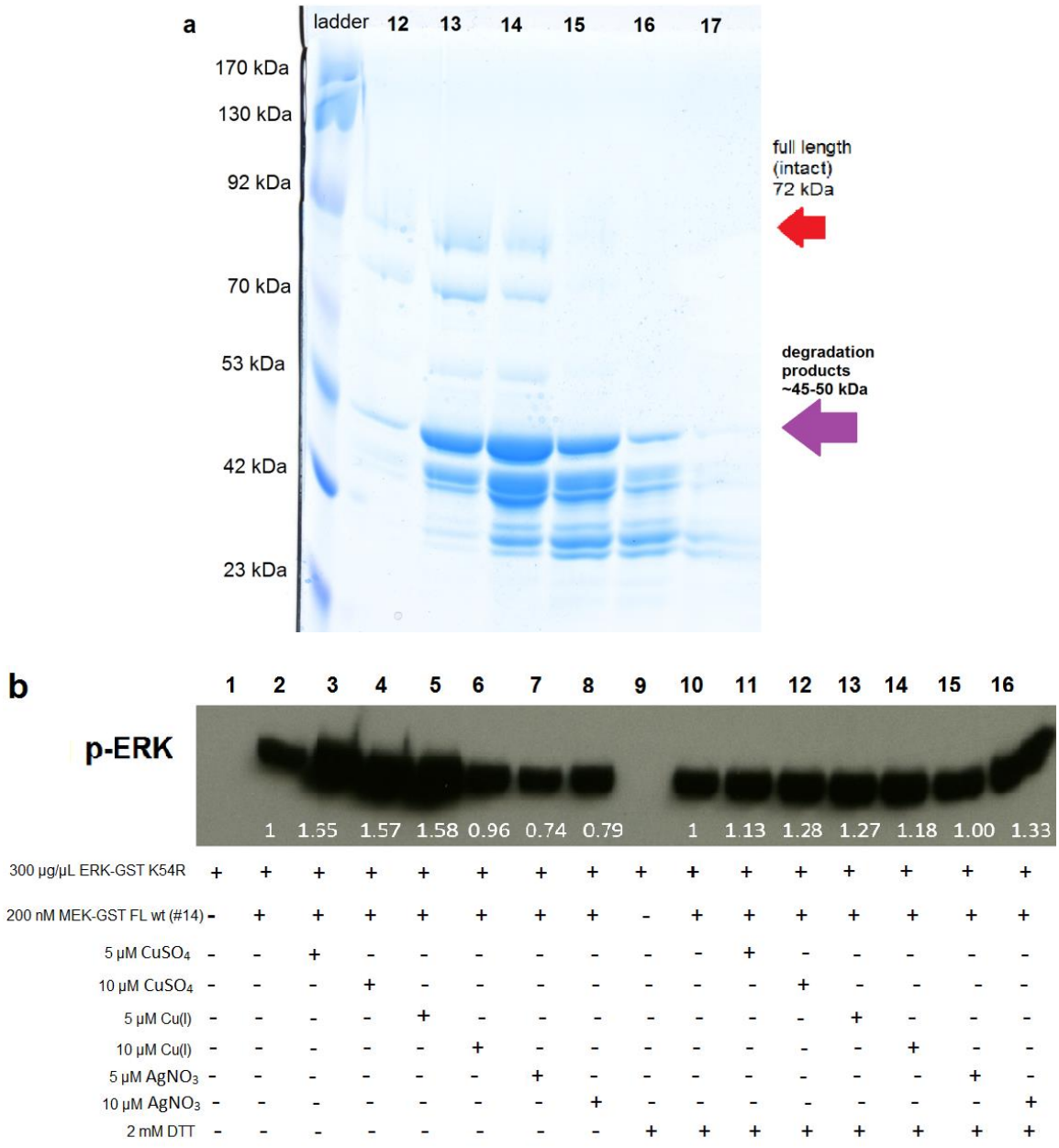

Figure 19. MEK1 FL wt GST Fraction #14 analysis: (a) gel electrophoresis of S200 run of Fraction #14 where the upper bands (around MEK1 FL wt GST's kDa) are only present in fractions 12-14 and (b) Western blot of Fraction #14's combined and concentrated sample, which was consistent with the initial Western dot blot results for Fraction #14 (Figure 17), activation observed with Cu^{2+} and Cu(I) without DTT and Ag^{+} with DTT.

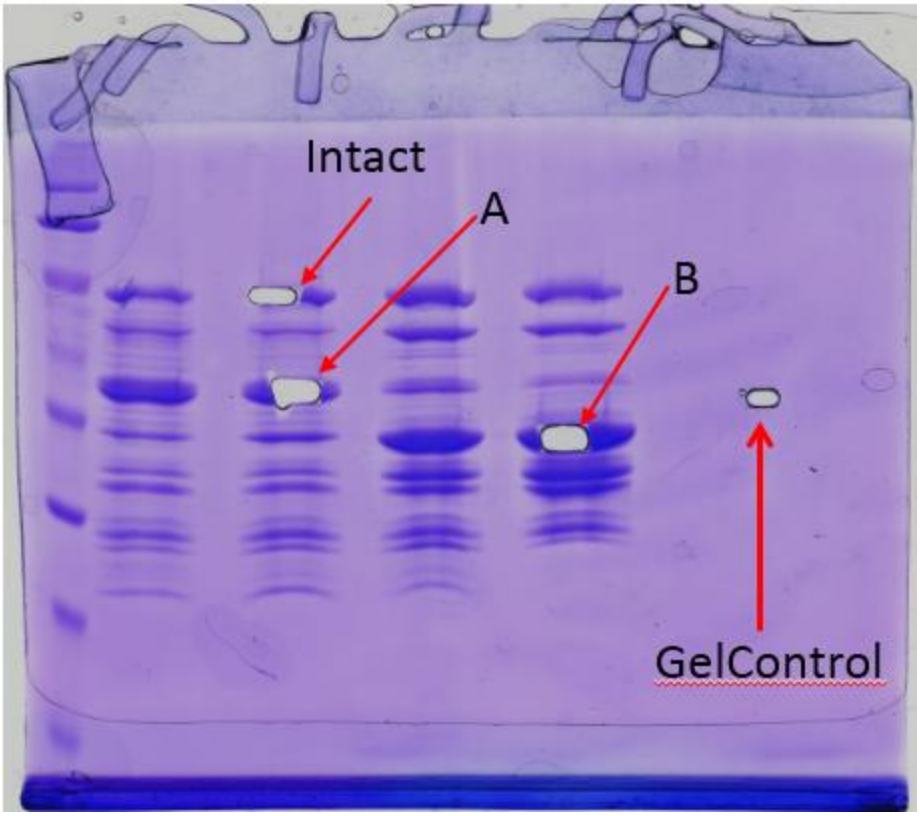

Figure 20. The mass spectrometry gel after destaining for 2 hours in destain solution. The bands were selected (A and B) to compare with the full length (intact) protein. A gel control was taken to subtract from background signal caused by the acrylamide gel.

Since both of these degradation bands did not include any of the observed sites C207, H188, and D208's backbone from the crystal structure and these sites were far upstream from the last residue, 152, within the degradation band. Another interaction site must be present. After returning to the MEK1 Cu-bound structure and scanning MEK1's residues 45-152, another Cu-anomalous signal was observed at the C121 site (Figure 21a). This was not thought to be a true interaction within the structure, since this anomalous density was only present in one subunit; however, upon overlaying both subunits within the asymmetric subunit, the C121 and K185 side chains did line up. This led to the conclusion that while the anomalous density was not present in the other subunit, the presence of Cu was biologically relevant. This biological relevancy comes from the side chains being in the same conformation for both subunits within the asymmetric unit. This was further confirmed by overlaying the apo- and Cu-bound structures, where drastic conformational changes occur for H184 and K185 with C121 remaining in the same position (Figure 21b).

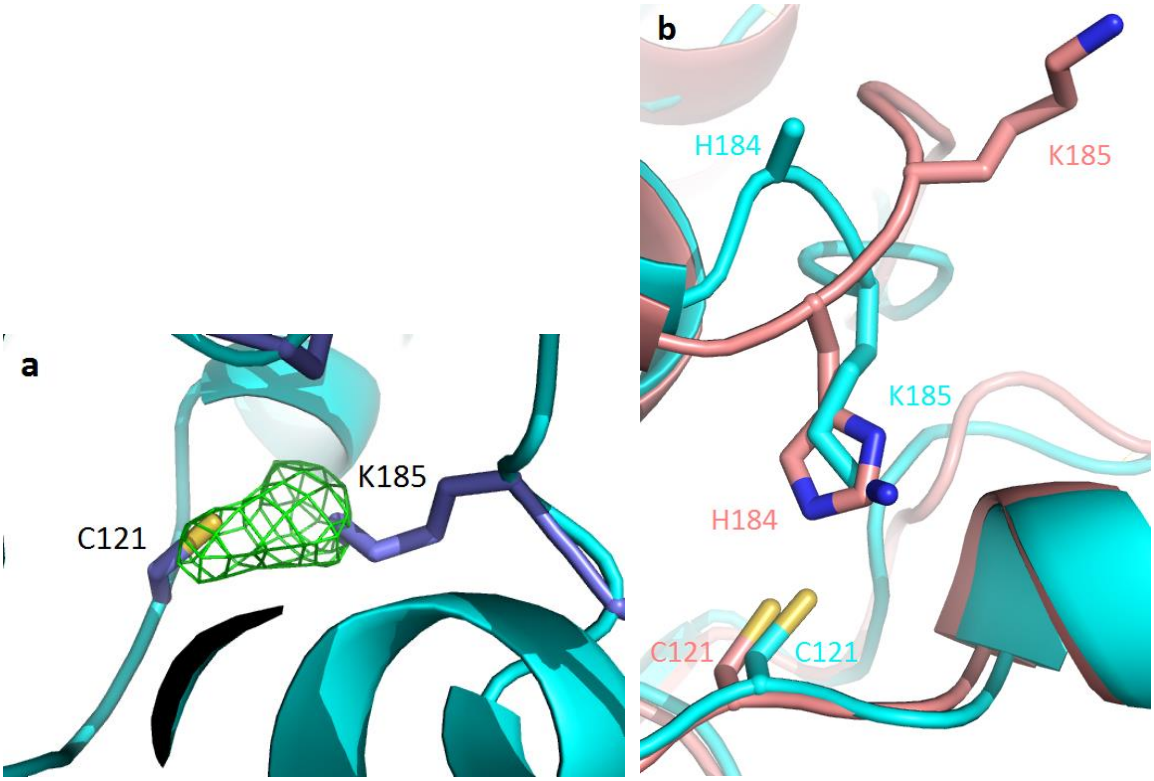

Figure 21. Analysis of the C121 site: (a) the Cu-anomalous signal map showing an interaction occurring at the C121 site, which is similar to the C207 site's anomalous signal density, and interacting with the K185 and (b) overlay comparison between apo-(pink) and Cu-bound(cyan) MEK1 structures at the C121 site.

Furthermore, the K185 and H184 are only a few residues downstream from the H188 position, which is involved in coordinating copper near the kinase's active site. Given that these two sites are in close proximity, it is possible that one is a regulatory site, while the other affects activity depending on the presence or absence of copper at the other site. The flipping of H188 would affect the residues on that same strand, ie. K185 and H184. Since the H188 is part of the regulatory HRD motif, it is likely that this histidine is aiding in chelating the copper near the active site, similar to its effect when magnesium (Mg^{2+}) is present for ATP hydrolysis. The C121 site's copper interaction could then be rotating as a subsequent action of the H188 flipping inward toward its Cu coordination site causing the change in kinase activity. These two Cu sites in combination with the oxidation state of the Cu present could be the key factors affecting the kinase activity of MEK1.

Summary and Conclusions

The X-ray structures reveal that MEK1 as in an inactive kinase conformation with the DFG-Phe flipped in and the square planar conformation of the Cu ion leads to the conclusion that the metal is in the Cu^{2+} oxidation state. *In vitro* studies using bacterially expressed homogeneously purified MEK1 is inhibited by Cu and Ag, while crudely purified MEK1 is activated by these metals. The requirement of reducing agent suggests that either the kinase (MEK1) or the metal (Cu) need to be or are being reduced in order for the activation to occur. From these data, the current model appears to be that a MEK1

interacting factor (a piece of MEK1 or another protein) mediates the Cu activation through a different site than the inhibitory site observed in the crystals. Thus the two Cu interaction sites, C207 and C121, have different effects on MEK1's activity. For the highly purified recombinant MEK1, it is plausible that there is a certain threshold concentration for Cu^{2+}, where its concentration causes a switch from activation and inhibitory. The number of Cu atoms binding and the oxidation state of the metal appear to be key components to the effect metal binding on MEK1 activity. Given that MEK1 is a kinase within an extremely efficient kinase cascade pathway, activity can increase to unsafe levels rather quickly if unregulated. This could be a potential feedback loop for inhibition of high levels of MEK1 activity.

Future Directions

This study has been able to address some questions about the mechanism for how copper interacts and affects MEK1, but has also resulted in new questions about how MEK1 could interact with other metals such as Ag to mediate both kinase activation and inhibition. The Cu interaction characterization, including both the C207 and C121 sites, should be completed with an EPR or XAS assay, which can detect the minute changes that occur from the binding event when a single element (Cu) binds to MEK1. While the Cu binding events greatly affect activity, they are not large binding events, like ATP binding to the active site, thus its small binding event is hard to detect unless using hypersensitive techniques. It would be helpful to further confirm the oxidation state of Cu when bound/interacting with MEK1, to perhaps tease out the differences between Cu^{+} and Cu^{2+} binding to MEK1, although Cu^{+} binding should be mimicked with Ag^{+} which is technically easier to produce in homogeneous form. Findings in the Ag^{+} interactions in this study hints that further studies should be pursued to determine the activation capacity of Ag^{+} compared to Cu. Metals binding to the active site can be a way to probe this location through conformational changes and allow for certain inhibitors to bind stronger and in specific ways. By better understanding how metal binding affects MEK1 activity, new inhibitors may be designed for MEK1.

References

(1) Melanoma Research Foundation. Melanoma fact sheet, 2016. Melanoma Research Institute. http://www.melanoma.org/sites/default/files/2016 melanomafactsheet.pdf (accessed Apr 20, 2016).

(2) Geller, A. C.; Clapp, R. W.; Sober, A. J.; Gonsalves, L.; Mueller, L.; Christiansen, C. L.; Shaikh, W.; Miller, D. R. Melanoma epidemic: an analysis of six decades of data from the Connecticut Tumor Registry. *J. Clin. Onco.* **2013**, *31* (33), 4172–4178.

(3) Brady, D. C.; Crowe, M. S.; Turski, M. L.; Hobbs, G. A.; Yao, X.; Chaikuad, A.; Knapp, S.; Xiao, K.; Campbell, S. L.; Thiele, D. J.; Counter, C. M. Copper is required for oncogenic BRAF signaling and tumorigenesis. *Nature.* **2014**, *509* (7501), 492–496.

(4) Wellbrock, C.; Karasarides, M.; Marais, R. The RAF proteins take centre stage. *Nat. Rev. Mol. Cell Biol.* **2004**, *5* (11), 875–885.

(5) Roskoski, Jr., R. ERK1/2 MAP kinases: structure, function, and regulation. *Pharmacol. Res.* **2012** *66* (2), 105–143.

(6) O'Connor, C. M. & Adams, J. U. 4.4 Receptor tyrosine kinases regulate cell growth, differentiation, and survival. *Essentials of Cell Biology* [Online]; Scitable by Nature Education: Cambridge, MA, 2010. https://www.nature.com/scitable/ebooks/essentials-of-cell-biology-14749010/118241359 (accessed Feb 13, 2017).

(7) Nazarian, R.; Shi, H.; Wang, Q.; Kong, X.; Koya, R. C.; Lee, H.; Chen, Z.; Lee, M.-K.; Attar, N.; Sazegar, H.; Chodon, T.; Nelson, S. F.; McArthur, G.; Sosman, J. A.; Ribas, A.; Lo, R. S. Melanomas acquire resistance to B-RAF(V600E) inhibition by RTK or N-RAS upregulation. *Nature.* **2010**, *468* (7326), 973–977.

(8) Ohren, J. F.; Chen, H.; Pavlovsky, E.; Whitehead, C.; Zhang, E.; Kuffa, P.; Yan, C.; McConnell, P.; Spessard, C.; Banotai, C.; Mueller, W. T.; Delaney, A.; Omer, C.; Sebolt-Leopold, J.; Dudley, D. T.; Leung, I. K.; Flamme, C.; Warmus, J.; Kaufman, M.; Barrett, S.; Tecle, H.; Hasemann, C. A. Structures of human MAP kinase kinase 1 (MEK1) and MEK2 describe novel noncompetitive kinase inhibition. *Nat. Struct. Mol. Biol.* **2004**, *11* (12), 1192-1197.

(9) Meier, C.; Brookings, D. C.; Ceska, T. A.; Doyle, C.; Gong, H.; McMillan, D.; Saville, G. P.; Mushtaq, A.; Knight, D.; Reich, S.; Pearl, L. H.; Powell, K. A.; Savva, R.; Allen, R. A. Engineering human MEK-1 for structural studies: a case study of combinatorial domain hunting. *J. Struct. Biol.* **2012**, *177* (2), 329-334.

(10) Ung, P. M.-U.; Schlessinger, A. DFGmodel: predicting protein kinase structures in inactive states for structure-based discovery of type-II inhibitors. *ACS Chem. Biol.* **2015**, *10* (1), 269-278.

(11) Melnik, M.; Ondrejovic, G.; Kabesova, M.; Baloghova, Z.; Broskovicova, A. *Heterometallic coordination copper (II) compounds: classification of analysis of crystallographic and structural data*; Nova Science Publishers, Inc.: Huntington, NY, 1999; pp 10–47. https://books.google.com/books?id=Oc3RXIFX2_YC&pg =PA46&lpg=PA46&dq=(11)+Melnik,+M.+Heterometallic+coordination+ copper+(II)+compounds:+classification+of+analysis+of+crystallographic+and +structural+data&source=bl&ots=ggBkjgKpg3&sig=SsjubSIkpzWiyFq_

xXCW83sKPRk&hl=en&sa=X&ved=0ahUKEwiEn66ttdPTAhXDQCYKHVsmDIcQ6AEIJzAA#v=onepage&q=(11)%20Melnik%2C%20M.%20Heterometallic%20coordination%20copper%20(II)%20compounds%3A%20classification%20of%20analysis%20of%20crystallographic%20and%20structural%20data&f=false (accessed October 30, 2016).

(12) Cheung, P. M.; Berger, R. F.; Zakharov, L. N.; Gilbertson, J. D. Square planar Cu(I) stabilized by a pyridinediimine ligand. *Chem. Commun.* **2016**, *52* (22), 4156-4159.

(13) Kornev, A. P.; Haste, N. M.; Taylor, S. S.; Eyck, L. F. T. Surface comparison of active and inactive protein kinases identifies a conserved activation mechanism. *Proc. Natl. Acad. Sci. U.S.A.* **2006**, *103* (47), 17783-17788.

(14) Oruganty, K.; Talathi, N.S.; Wood, Z.A.; Kanna, N. Identification of a hidden strain switch provides clues to an ancient structural mechanism in protein kinases. *Proc. Natl. Acad. Sci. U.S.A.* **2013**, *110* (3), 924-929.

(15) Read, R. J. Protein Crystallography Course. http://wwwstructmed.cimr.cam.ac.uk/course.html (Accessed October 25, 2016), Molecular Replacement.

(16) Goettel, J. A.; Liang, D.; Hilliard, V. C.; Edelblum, K. L.; Broadus, M. R.; Gould, K. L.; Hanks, S. K.; Polk, D. B. KSR1 is a functional protein kinase capable of serine autophosphorylation and direct phosphorylation of MEK1. *Exp. Cell Res.* **2011** *317* (4), 452–463.

(17) Wang, A.-X.; Qi, X.-Y. Targeting RAS/RAF/MEK/ERK signaling in metastatic melanoma. *IUBMB Life.* **2013**, *65* (9), 748–758.

(18) Mcarthur, G. A. Combination therapies to inhibit the RAF/MEK/ERK pathway in melanoma: we are not done yet. *Front.Oncol.* **2015**, *5*, 161.

Appendices

Appendix 1. Enzyme-Linked ImmunoSorbent Assay, Comparison of activity counts between (a) MEK1 FL wt and (b) MEK1 FL DD at various concentrations. As the concentration positively increases so do the activity levels for both untagged constructs**.** The difference occurs when phosphomimetic MEK1 construct (MEK1 FL DD) is tested and has higher activity counts (~45x) at all concentrations.

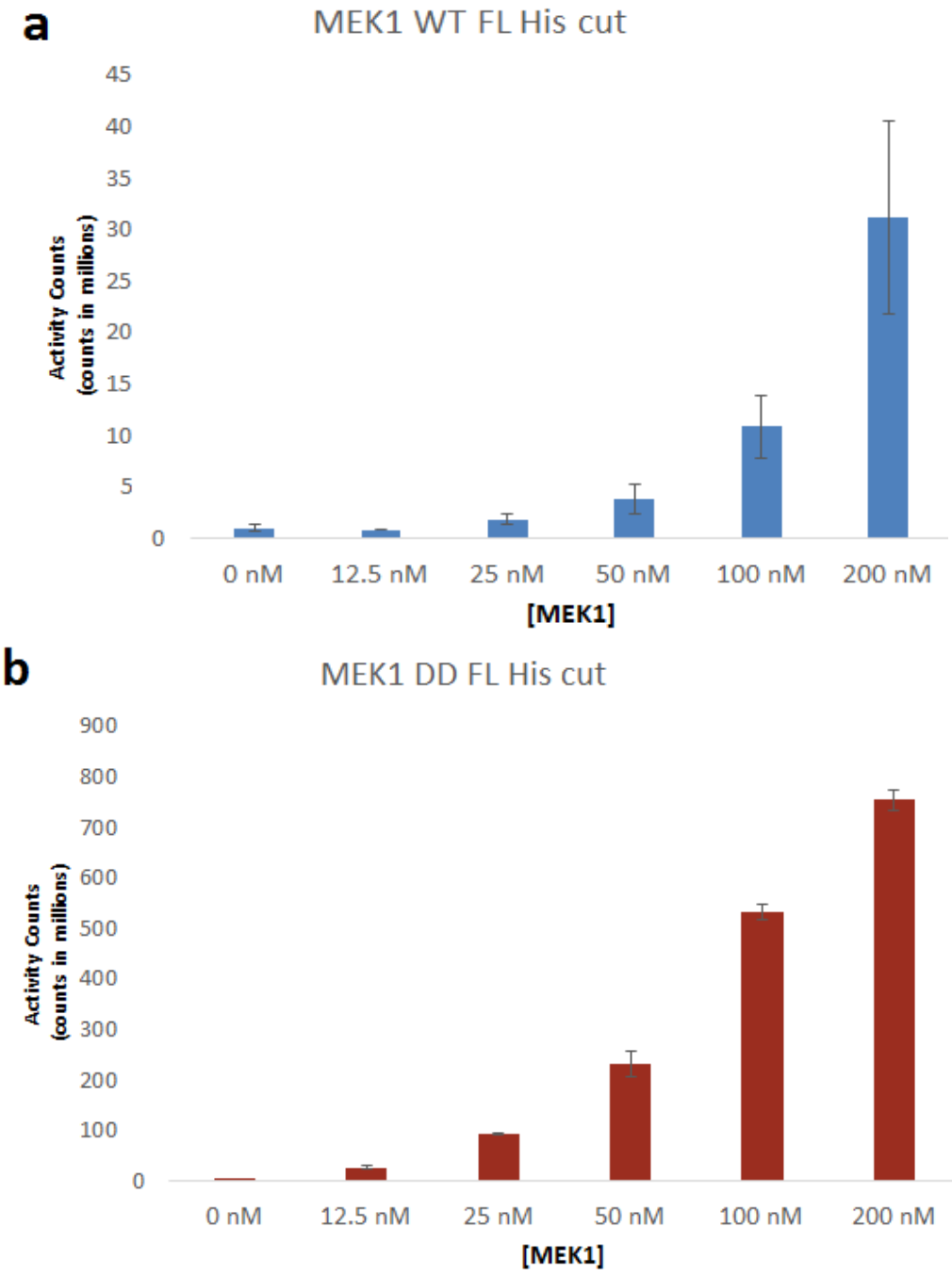

Appendix 2. Acrylamide Gel Electrophoresis, Comparison of a MEK-6His cut FL wt purification and MEK-GST FL wt purification. Both of these gels are after the final Superdex S200 sizing run. (a) MEK-6His cut FL wt has a singular clean set of bands at the correct molecular weight (44 kDa). (b) MEK-GST FL wt has the top band of FL intact MEK-GST (72 kDa) with multiple lower bands. These lower bands are degradation products caused by the GST tag. The degradation products are various pieces of the MEK-GST FL wt at the various lower molecular weights.